LETTER

doi:10.1038/nature21357

Synthetic essentiality of chromatin remodelling factor CHD1 in PTEN-deficient cancer

Di Zhao[1], Xin Lu[1]*, Guocan Wang[1]*, Zhengdao Lan[1], Wenting Liao[1], Jun Li[2], Xin Liang[1], Jasper Robin Chen[1], Sagar Shah[1], Xiaoying Shang[1], Ming Tang[2], Pingna Deng[1], Prasenjit Dey[1], Deepavali Chakravarti[1], Peiwen Chen[1], Denise J. Spring[1], Nora M. Navone[4], Patricia Troncoso[5], Jianhua Zhang[2], Y. Alan Wang[1] & Ronald A. DePinho[1]

Synthetic lethality and collateral lethality are two well-validated conceptual strategies for identifying therapeutic targets in cancers with tumour-suppressor gene deletions[1–3]. Here, we explore an approach to identify potential synthetic-lethal interactions by screening mutually exclusive deletion patterns in cancer genomes. We sought to identify 'synthetic-essential' genes: those that are occasionally deleted in some cancers but are almost always retained in the context of a specific tumour-suppressor deficiency. We also posited that such synthetic-essential genes would be therapeutic targets in cancers that harbour specific tumour-suppressor deficiencies. In addition to known synthetic-lethal interactions, this approach uncovered the chromatin helicase DNA-binding factor CHD1 as a putative synthetic-essential gene in PTEN-deficient cancers. In PTEN-deficient prostate and breast cancers, CHD1 depletion profoundly and specifically suppressed cell proliferation, cell survival and tumorigenic potential. Mechanistically, functional PTEN stimulates the GSK3β-mediated phosphorylation of CHD1 degron domains, which promotes CHD1 degradation via the β-TrCP-mediated ubiquitination–proteasome pathway. Conversely, PTEN deficiency results in stabilization of CHD1, which in turn engages the trimethyl lysine-4 histone H3 modification to activate transcription of the pro-tumorigenic TNF–NF-κB gene network. This study identifies a novel PTEN pathway in cancer and provides a framework for the discovery of 'trackable' targets in cancers that harbour specific tumour-suppressor deficiencies.

Prostate cancer is the second leading cause of cancer-related death for men in the United States, with 180,890 new cases and 26,120 deaths annually (NCI SEER 2016; http://seer.cancer.gov/csr/1975_2013/). Up to 70% of primary prostate tumours show loss of heterozygosity at the *PTEN* locus[4]. In mouse models, prostate-specific deletion of *Pten* ($Pten^{pc-/-}$) results in prostatic intraepithelial neoplasia, which may progress to high-grade adenocarcinoma after a long latency period[5], a pattern consistent with the loss of *PTEN* acting as a key initiation event in prostate cancer development. To date, therapeutic targeting of the PTEN–PI3K–AKT pathway has yielded meagre clinical benefit, prompting continued efforts to identify obligate effectors of this important pathway in order to identify effective therapeutic targets for PTEN-deficient cancers.

The notion of targeting synthetic-lethal vulnerabilities in cancer has been validated in the treatment of cancers that harbour specific loss-of-function mutations[1,6]. One celebrated example is the effectiveness of poly(ADP)-ribose polymerase (PARP) inhibitors in BRCA-deficient tumours[2,7]. More recently, collateral lethality has emerged as another target-discovery strategy for cancers harbouring tumour-suppressor gene deletions that also delete neighbouring genes encoding functionally redundant yet essential activities, thereby creating cancer-specific vulnerabilities[3,8]. Genomic analyses have also been helpful in identifying functional interactions of components in specific pathways that show mutually exclusive patterns of genomic alterations. Such epistatic patterns include components of the retinoblastoma (Rb) or p53 pathways, in which alterations in one gene in the pathway typically alleviates genetic pressure to alter another driver in the same pathway, consistent with minimal additional selective advantage to the cancer cell[9,10].

Using The Cancer Genome Atlas (TCGA) database, we sought to establish and validate an approach for identifying potential synthetic-lethal interactions in cancer by screening for mutually exclusive deletion patterns in the cancer genome. More specifically, we searched for genes that might occasionally be deleted in some cancers (that is, non-essential genes) but that are always retained in the context of deletion of a specific tumour suppressor, reasoning that the retained gene might be required for executing the cancer-promoting actions in the context of a specific tumour-suppressor deficiency (that is, a synthetic-essential gene). By extension, we posited that inhibition of these synthetic-essential genes would impair the survival and tumorigenic potential of cancer cells harbouring the specific tumour-suppressor deficiency. Here, we focused on prostate cancer owing to the frequent and early deletion of the PTEN tumour suppressor and the paucity of actionable 'oncogene' targets in prostate cancer.

The well established synthetic-lethal interaction of BRCA1 and PARP1 provides a measure of validation for our approach, since a mutually exclusive deletion pattern of BRCA1 and PARP1 is readily observed in the prostate cancer TCGA database (Extended Data Fig. 1a). Similarly, consistent with preclinical and clinical studies suggesting that PTEN deficiency sensitizes prostate, colorectal and endometrial cancer cells to PARP inhibitors[11,12], we observed a synthetic-essential relationship between PTEN and PARP1 (Extended Data Fig. 1b). Another mutually exclusive deletion pattern in prostate cancer points to an interaction between PTEN and polo-like kinase 4 (PLK4) (Extended Data Fig. 1b). This observation aligns well with the single-agent anti-tumour activity of the PLK4 inhibitor CFI-400945 and its capacity to induce the regression of *PTEN*-deficient cancers, compared with *PTEN*-intact cancer cells[13]. Together, these circumstantial data prompted us to speculate that druggable essential dependencies (synthetic-essential genes) of specific tumour-suppressor gene deficiencies might be uncovered by scanning the patterns of cancer genome deletions.

Large-scale genomic analyses of TCGA and other prostate cancer databases identified *CHD1* (5q21 locus) as a locus that is deleted in some human prostate cancer cases (7–10%)[14–16], but is consistently retained in *PTEN*-deficient prostate cancer (Fig. 1a and Extended Data Fig. 1c). In addition, the pattern of mutual exclusivity with *PTEN* deletion was observed for CHD1 but not for other CHD homologues (Extended Data Fig. 1d). The PTEN–CHD1 relationship was reinforced by the strong negative correlation observed between CHD1 and PTEN

[1]Department of Cancer Biology, The University of Texas MD Anderson Cancer Center, Houston, Texas 77030, USA. [2]Department of Genomic Medicine, The University of Texas MD Anderson Cancer Center, Houston, Texas 77030, USA. [3]Institute for Applied Cancer Science, The University of Texas MD Anderson Cancer Center, Houston, Texas 77054, USA. [4]Department of Genitourinary Medical Oncology, The University of Texas MD Anderson Cancer Center, Houston, Texas 77030, USA. [5]Department of Pathology, The University of Texas MD Anderson Cancer Center, Houston, Texas 77030, USA. *These authors contributed equally to this work.

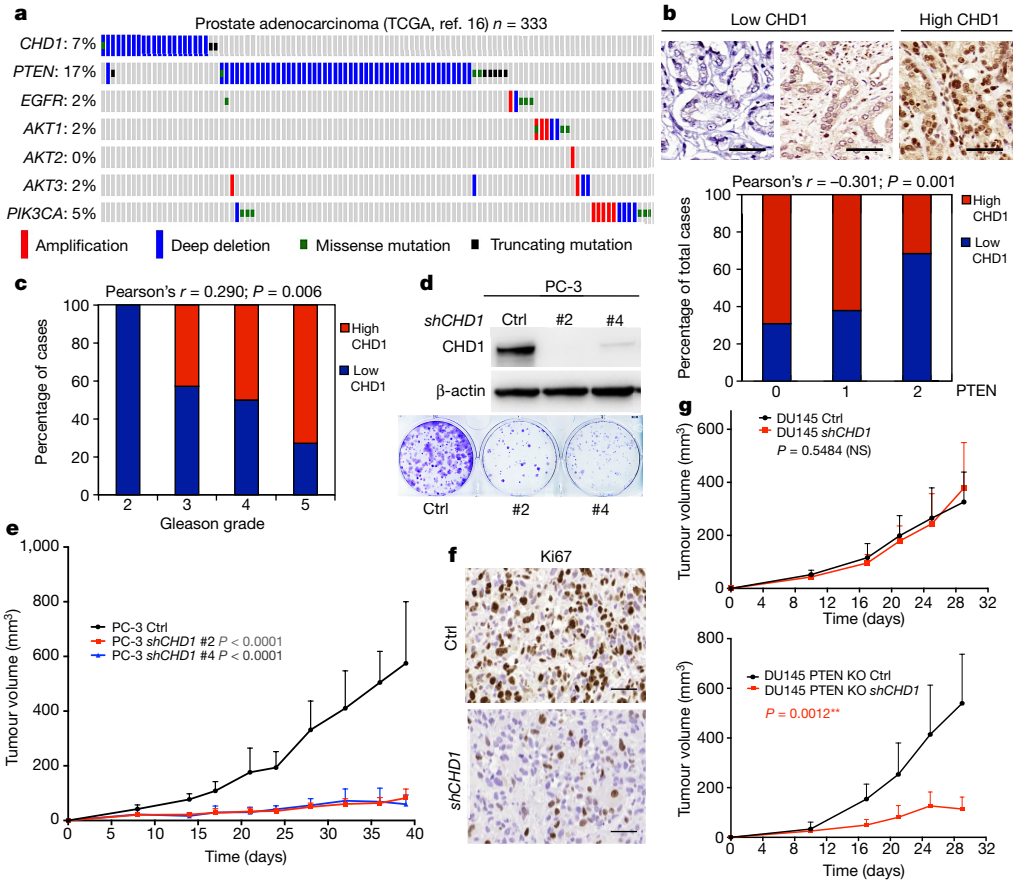

Figure 1 | Knockdown of CHD1 inhibits tumour growth of PTEN-null prostate cancer. a, Genomic alterations of *CHD1* and genes in the PTEN–AKT pathway in TCGA prostate cancer database ($n = 333$)[16]. **b**, Representative images of CHD1 expression, and the negative correlation between CHD1 and PTEN expression in human prostatic hyperplasia and cancer samples ($n = 127$). **c**, Distribution of CHD1 expression in human prostate cancer samples with different Gleason grades ($n = 90$). Pearson correlation coefficient and two-tailed *P* value are shown. **d**, Immunoblots of lysates and colony-formation assays generated from shRNA-mediated *CHD1*-knockdown and control (ctrl) PC-3 cells. See Methods for details of *shCHD1* #2 and #4. Representative data of triplicate experiments are shown. **e**, Measurement of subcutaneous tumour growth of *CHD1*-knockdown and control PC-3 cells. Control, $n = 10$; *shCHD1* #2, $n = 10$; *shCHD1* #4, $n = 8$. **f**, Representative images of Ki67 staining of subcutaneous tumour tissues generated from samples in **e**. **g**, Measurement of subcutaneous tumour growth of *CHD1*-knockdown PTEN-intact or -deficient DU145 cells. *PTEN*-knockout (KO) *shCHD1* $n = 5$; other groups $n = 6$ for each. Error bars in **e** and **g** indicate s.d. *P* values were determined by two-tailed *t*-test. NS, not significant. Scale bars, 50 μm (**b**, **f**).

expression by immunohistochemistry analysis of 127 prostatic hyperplasia and cancer tissue microarray samples ($P = 0.001$, Fig. 1b and Extended Data Fig. 2a, b). CHD1 deletion *per se* does not appear to play a significant role in prostate cancer development, as indicated by the lack of neoplasia in a tissue recombinant model using mouse prostate epithelial progenitor or stem cells in which *CHD1* is deleted[17]. Rather, CHD1 expression correlates positively with a high Gleason grade ($P = 0.006$, Fig. 1c and Extended Data Fig. 2c) and is increased in neoplastic *Pten*-deficient mouse prostatic epithelium compared to wild-type controls (Extended Data Fig. 2d, e). Collectively, these observations prompted us to consider the possibility that CHD1 may be required for the progression of prostate cancer driven by the loss of PTEN.

To test the above hypothesis, we carried out short hairpin RNA (shRNA)-mediated depletion or CRISPR-directed nullizygous mutation of *CHD1* in four PTEN-deficient prostate cancer cell lines (shRNA depletion in human LNCaP and PC-3 prostate cancer cell lines, and in mouse Pten/Smad4-null and PtenCaP8 prostate cancer cell lines; CRISPR nullizygous mutation in the LNCaP cell line). In these models, *CHD1* suppression inhibited colony formation and induced cell death (Fig. 1d and Extended Data Fig. 2f–j), but it had a minimal effect on cell migration (Extended Data Fig. 2k). Moreover, *CHD1* depletion attenuated the growth of tumours derived from PC-3 and LNCaP cells *in vivo* (Fig. 1e and Extended Data Fig. 2l, m) and, correspondingly, these tumours exhibited a marked reduction in cell proliferation (as measured by Ki67 levels) and increase in apoptosis (as measured by caspase-3 levels) (Fig. 1f and Extended Data Fig. 2n). Similarly, administration of a short interfering RNA targeting *CHD1* (*siCHD1*) in established *PTEN*-deficient patient-derived xenograft (PDX) tumours attenuated tumour progression (Extended Data Fig. 2o, p). However, *CHD1* depletion had a minimal effect on colony formation or tumour growth of the *PTEN*-intact prostate cancer cell lines 22Rv1, RWPE-2 and DU145 (Fig. 1g and Extended Data Fig. 3a–d). By contrast, CRISPR-mediated knockout of *PTEN* in DU145 cells sensitized the cells to *CHD1* depletion both *in vitro* and *in vivo* (Fig. 1g and Extended Data Fig. 3c, d). Together, these data support the view that *CHD1* is a synthetic-essential gene that is required for tumour growth of *PTEN*-null prostate cancer, a functional relationship consistent with the mutually exclusive pattern of *PTEN* and *CHD1* deletions.

Exploration of the functional relationship between PTEN and CHD1 revealed that PTEN re-expression in *PTEN*-null prostate cancer cell lines led to a substantial decrease in levels of CHD1 protein, but not mRNA (Fig. 2a and Extended Data Fig. 3e). Correspondingly, transient ectopic expression of GFP–PTEN suppressed *CHD1* in PC-3 cells at the single-cell level (Fig. 2b). Time-course studies revealed that treatment with the AKT inhibitor MK2206 reduced CHD1 protein levels over a 6-h period (Fig. 2c) and that PTEN re-expression reduced the half-life of CHD1 protein (Extended Data Fig. 3f), supporting a role for

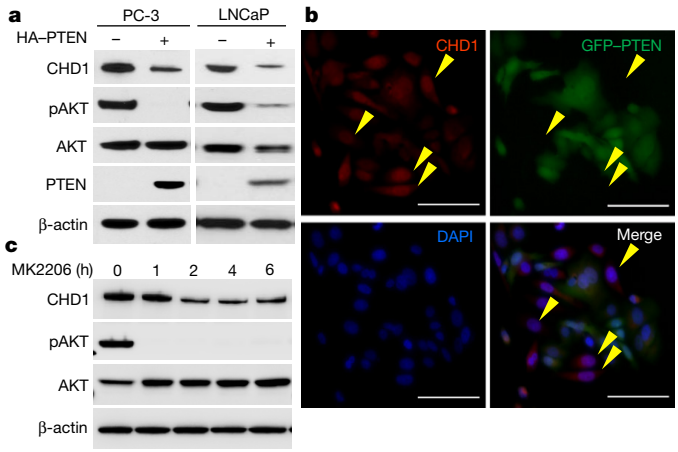

Figure 2 | PTEN inhibits CHD1 by decreasing its protein stability. **a**, Immunoblots of lysates generated from human PC-3 and LNCaP cells that overexpress PTEN. **b**, Co-staining of CHD1 and PTEN by immunofluorescence in PC-3 cells overexpressing GFP–PTEN. The yellow arrows indicate GFP–PTEN-negative cells. Scale bar, 100 μm. **c**, Immunoblot of CHD1 protein in LNCaP cells treated with 2 μM AKT inhibitor (MK2206). pAKT, Ser473-phosphorylated AKT. Representative data of triplicate experiments are shown.

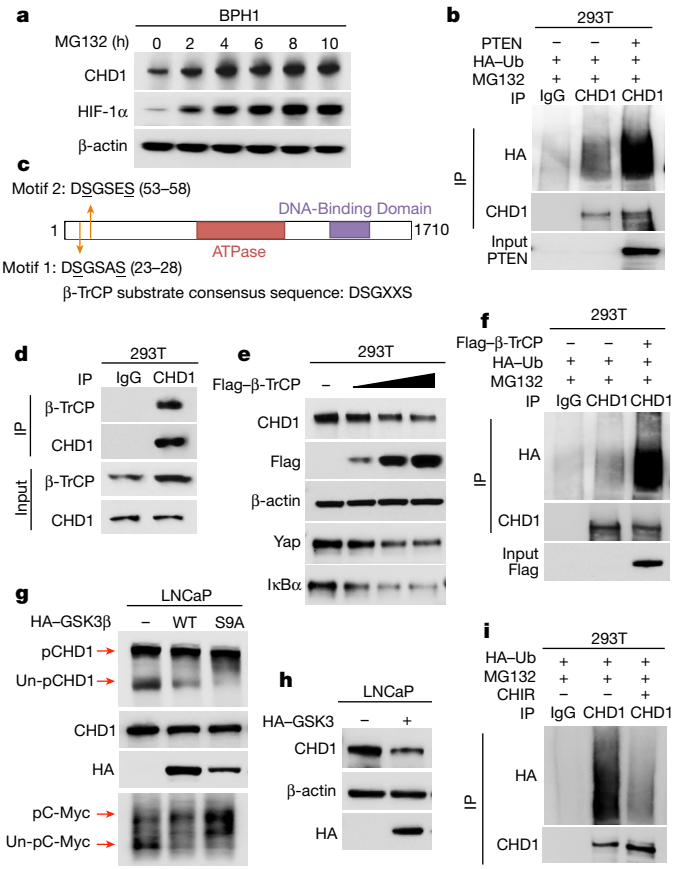

Figure 3 | PTEN promotes CHD1 degradation through $SCF^{β\text{-}TrCP}$-mediated ubiquitination–proteasome pathway. **a**, Detection of CHD1 in BPH1 cells treated with 10 μM MG132 (HIF-1α was used as a positive control). **b**, 293T cells were transfected with PTEN and haemagglutinin (HA)-tagged ubiquitin and then treated for 8 h with MG132. Immunoprecipitation (IP) of endogenous CHD1; CHD1 and HA were detected by immunoblot. **c**, Schematic diagram of two β-TrCP-binding motifs (DSGXXS) in CHD1. **d**, Co-immunoprecipitation using an anti-CHD1 antibody, followed by detection of β-TrCP via immunoblot. **e**, Immunoblot of CHD1 in 293T cells overexpressing Flag-tagged β-TrCP (Yap and IκBα as positive controls). **f**, 293T cells were transfected with Flag-tagged β-TrCP and HA-tagged ubiquitin; endogenous CHD1 was immunoprecipitated and CHD1 ubiquitination was detected. **g**, HA-tagged wild-type (WT) and constitutively active mutant (S9A) GSK3β were transfected into LNCaP cells and phosphorylated and unphosphorylated CHD1 proteins were separated using phos-tag gel by immunoblot. Total CHD1 protein was used as a loading control, C-Myc as a positive control. **h**, Immunoblot of CHD1 in LNCaP cells transfected with HA-tagged GSK3β. β-actin was used as a loading control. **i**, HA-tagged ubiquitin was transfected into 293T cells, followed by treatment with 2 μM CHIR (at 24 h) and 10 μM MG132 (at 8 h) and detection of CHD1 ubiquitination by immunoprecipitation and immunoblot. Representative data of triplicate experiments are shown.

the PTEN–AKT axis in the control of CHD1 protein levels. Moreover, CHD1 was more stable in *PTEN*-deficient cells than in *PTEN*-intact cells (Extended Data Fig. 3f–h). To explore the mechanisms governing CHD1 protein levels, we treated the *PTEN* wild-type benign prostatic hyperplasia epithelial cell line BPH1 with the proteasome inhibitor MG132, resulting in the marked accumulation of CHD1 in a time-dependent manner (Fig. 3a). Moreover, endogenous CHD1 was modified by ubiquitination (Extended Data Fig. 4a) and PTEN overexpression greatly enhanced CHD1 ubiquitination (Fig. 3b). Together, these data suggest that CHD1 degradation is controlled through the ubiquitination–proteasome pathway in a PTEN-dependent manner.

To identify a specific E3 ligase that governs CHD1 protein stability, we performed consensus-sequence scanning of multiple E3 ligase interaction domains and identified two evolutionarily conserved putative β-TrCP consensus-binding motifs (DSGXXS) at the N terminus of CHD1—residues 23–28 (motif 1, DSGSAS) and 53–58 (motif 2, DSGSES) (Fig. 3c and Extended Data Fig. 4b). β-TrCP is an F-box protein that acts as the substrate-recognition subunit for the $SCF^{β\text{-}TrCP}$ (Skp1–Cullin1–F-box protein) E3 ubiquitin ligases, which mediate the ubiquitination and proteasomal degradation of various substrates, including β-catenin, Yap and IKB[18–20]. The CHD1–β-TrCP link was confirmed by documentation of the endogenous interaction of CHD1 and β-TrCP using co-immunoprecipitation (Fig. 3d) and by the fact that β-TrCP overexpression resulted in reduced CHD1 protein levels and enhanced CHD1 ubiquitination (Fig. 3e, f and Extended Data Fig. 4c). Conversely, shRNA-mediated depletion of β-TrCP caused accumulation of CHD1 and inhibited its ubiquitination (Extended Data Fig. 4d, e). To investigate whether the β-TrCP binding motifs of CHD1 were involved in the regulation of CHD1 protein stability, we introduced wild-type V5-peptide-tagged CHD1 and two β-TrCP-binding motif mutants (DAGXXA) into BPH1 cells, and then analysed the half-life, ubiquitination and β-TrCP interaction of CHD1. These experiments established that motif 2 (DSGSES) serves as the major β-TrCP-binding motif that contributes to CHD1 ubiquitination and degradation (Extended Data Fig. 4f–h).

β-TrCP recognizes and interacts specifically with phosphorylated substrates[21]. Our analysis of CHD1 showed that both β-TrCP-binding motifs harbour a GSK3β consensus sequence (SXXXS; Extended Data Fig. 4i). Since GSK3β is a direct target of AKT and is inhibited upon AKT activation, we anticipated that PTEN loss would impair GSK3β activity, resulting in decreased CHD1 phosphorylation and subsequent ubiquitination. In line with this possibility, overexpression of GSK3β and its constitutively active mutant (S9A) in LNCaP cells increased the phosphorylation of CHD1 (Fig. 3g). This connection was reinforced by the observed endogenous interaction between GSK3β and CHD1 (Extended Data Fig. 4j), as well as by a decrease in CHD1 levels reduced by enforced expression of GSK3β (Fig. 3h). Finally, treatment with CHIR-99021, an inhibitor of GSK3β, decreased CHD1 ubiquitination (Fig. 3i) and blocked the negative effect of PTEN expression on CHD1 protein stability (Extended Data Fig. 4k). Together, these data establish that the PTEN–AKT–GSK3β pathway regulates CHD1 degradation via the β-TrCP-mediated ubiquitination–proteasome pathway.

Trimethylation of histone H3 at lysine 4 (H3K4me3) is associated with transcriptional activation and CHD1 selectively recognizes and

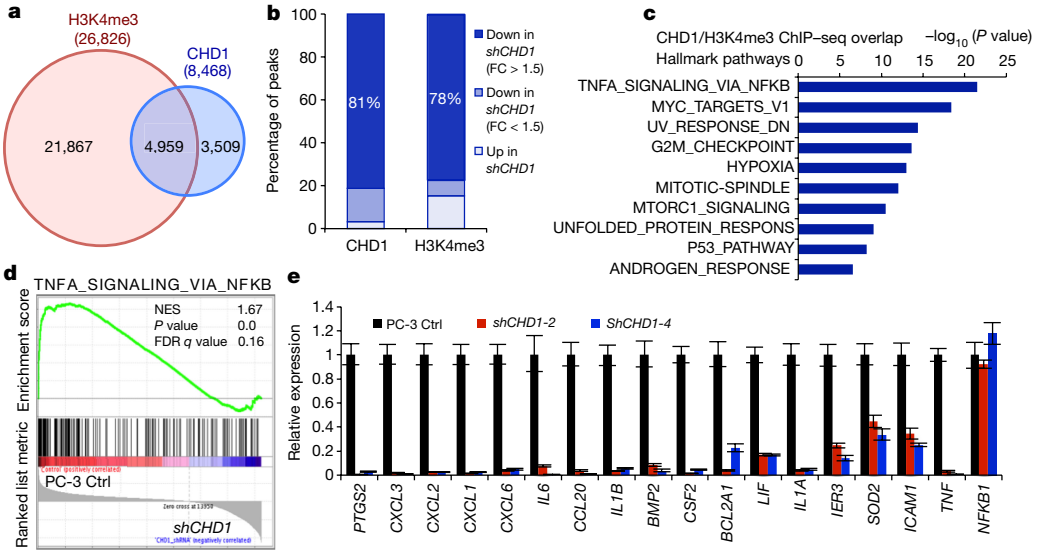

Figure 4 | CHD1 collaborates with H3K4me3 to activate gene transcription in the NF-κB pathway in PTEN-deficient prostate cancer. a, Venn diagrams showing the overlap of peak sets identified from the duplicate-merged CHD1 and H3K4me3 ChIP–seq in PC-3 cells. Blue circle, CHD1 peaks; red circle, H3K4me3 peaks. **b**, Percentage of decreased CHD1 or H3K4me3 ChIP–seq peaks in *CHD1*-knockdown PC-3 cells. FC, fold change. **c**, Top ten hallmark pathways exhibiting enrichment of CHD1 and H3K4me3 ChIP–seq overlap genes. A total of 50 MSigDB hallmark pathways emerged following ingenuity pathway analysis (IPA) 'core analysis'. Graph displays category scores as $-\log_{10}$ (*P* value) from Fisher's exact test. **d**, GSEA correlation of NF-κB signature with alternatively expressed genes in *CHD1*-knockdown PC-3 cells. Normalized enrichment score (NES), Nominal *P* value and false discovery rate *q* value of correlation are shown. **e**, Validation of CHD1-regulating genes in *CHD1*-knockdown PC-3 cells using qPCR. Data are mean ± s.d. of triplicate experiments.

binds to H3K4me3 to activate gene transcription[22]. In addition, CHD1 is involved in the maintenance of open chromatin and cooperates with H3K4me3 to control the pluripotency of mouse embryonic stem cells[23]. Correspondingly, co-immunoprecipitation studies in BPH1 cells confirmed that CHD1 binds to H3K4me3 (Extended Data Fig. 5a) and CHD1 depletion in LNCaP and PC-3 cells revealed a substantial reduction in the H3K4me3 mark (Extended Data Fig. 5b, c). To identify the downstream transcriptional targets and pathways of CHD1 and H3K4me3 in *PTEN*-null prostate cancer cells, we performed chromatin immunoprecipitation followed by sequencing (ChIP–seq) in control and *CHD1*-knockdown PC-3 cells. ChIP–seq identified a total of 8,468 CHD1-binding sites and 26,826 H3K4me3-enriched regions in control PC-3 cells, with 58.6% of CHD1 peaks overlapping with H3K4me3 peaks (Fig. 4a). In total, 81.4% of CHD1-binding sites showed reduced peak values in *CHD1*-depleted PC-3 cells, validating our experimental methodology (Fig. 4b and Extended Data Fig. 5d). Notably, 77.5% of the peak values of regions enriched for H3K4me3 were concomitantly diminished in *CHD1*-depleted PC-3 cells (Fig. 4b and Extended Data Fig. 5d), strongly supporting a role for CHD1 in H3K4me3 maintenance in prostate cancer. In addition, pathway analysis of either the genes concomitantly regulated by CHD1/H3K4me3 or the genes whose promoters are bound by CHD1 revealed a significant enrichment for genes involved in the TNF–NF-κB network (Fig. 4c, Extended Data Fig. 5e and Supplementary Table 1, 2).

Next, we performed microarray analysis in CHD1-depleted PC-3 and LNCaP cells (Supplementary Tables 3, 4). The expression profiles of these cells aligned with the above ChIP–seq data, confirming that TNF–NF-κB was the most downregulated hallmark pathway in CHD1-depleted cells (Fig. 4d and Extended Data Fig. 5f, g). Of the 30 most downregulated genes in *shCHD1* PC-3 cells, 10 were target genes of NF-κB (Extended Data Table 1). Notably, pathway-enrichment analysis showed that the TNF–NF-κB pathway is activated in *PTEN*-null mouse prostate tissue (Extended Data Fig. 5h), suggesting that regulation of the TNF–NF-κB network is linked to the PTEN–CHD1 axis.

NF-κB is a key regulator of inflammation and plays important roles in prostate cancer initiation and progression[24]. Blockade of NF-κB alone or in combination with anti-androgenic drugs suppresses tumour growth and metastasis in prostate cancer[25,26]. Downregulated genes in the TNF–NF-κB pathway that were identified by our microarray analysis include genes that control tumour cell proliferation (*PTGS2*) and apoptosis (*IER3*, *BCL2* and *SOD2*), as well as multiple cytokines that remodel the tumour microenvironment (multiple CXCL genes, *IL1* and *IL6*)[24] (Extended Data Fig. 5i). These gene expression results were further validated by quantitative real-time PCR (qPCR) (Fig. 4h and Extended Data Fig. 5j) and, upon analysis of clinical samples in the TCGA prostate cancer database, expression of these TNF–NF-κB pathway genes was positively correlated with CHD1 expression (Extended Data Fig. 6a). Although we identified many direct target genes of NF-κB, we did not observe changes in levels of total or activated NF-κB p65 on depletion of *CHD1* (Fig. 4h and Extended Data Fig. 6b). On the basis of CHD1 and H3K4me3 ChIP–seq data, all 90 downregulated genes in the TNF–NF-κB pathway can be subdivided into three categories: (1) genes that are bound by CHD1 and marked by H3K4me3 (41.1%), consistent with CHD1 having direct transcriptional control of these genes, presumably via its interaction with the H3K4me3 mark; (2) genes that are not bound by CHD1 but that exhibit decreased H3K4me3 enrichment upon CHD1 depletion (47.8%), possibly reflecting CHD1-directed maintenance of the H3K4me3 modification, which activates target transcription; and (3) genes neither bound by CHD1 nor marked by H3K4me3 (approximately 10%), suggesting that they are indirectly regulated by CHD1 and H4K4me3 (Extended Data Fig. 6c and Extended Data Table 2). Thus, the majority (88.9%) of downregulated TNF–NF-κB pathway genes are under the transcriptional control of CHD1, either directly or through its maintenance of the H3K4me3 modification. Finally, consistent with PTEN–CHD1–NF-κB pathway epistasis, the enforced addition of several CHD1-target genes, such as *PTGS2*, *BMP2* and *CSF2*, rescued colony formation in prostate cancer cells deficient in both PTEN and CHD1 (Extended Data Fig. 6d).

Together, our data demonstrate that the epigenetic regulator CHD1 represents a prime therapeutic target candidate in *PTEN*-deficient prostate cancer, validating our *in silico* approach to identifying synthetic-essential genes. Furthermore, our study identifies a novel PTEN pathway linking PTEN and chromatin-mediated regulation of the cancer-relevant NF-κB network. Specifically, mechanistic analyses

identified the PTEN–AKT–GSK3β–β-TrCP-mediated degradation of CHD1 via the ubiquitination–proteasome pathway (Extended Data Fig. 7a). In cancer, *PTEN* deficiency stabilizes CHD1, which engages and maintains the H3K4me3 modification to activate the expression of cancer-promoting genes, including those involved in the NF-κB network, which is known to promote prostate cancer progression (Extended Data Fig. 7b). In addition to prostate cancer, the mutually exclusive deletion pattern of *PTEN* and *CHD1* is also present in breast and colorectal adenocarcinoma (Extended Data Fig. 7c). To evaluate any potential roles for CHD1 in breast cancer, shRNA-mediated depletion was induced in two *PTEN*-deficient (BT-549 and MDA-MB-468) and two *PTEN*-intact (MDA-MB-231 and T47D) breast cancer cell lines. Consistent with the observations in prostate cancer, suppression of CHD1 inhibited the proliferation and tumour growth of *PTEN*-deficient breast cancer (Extended Data Fig. 7d–f), but had a minimal effect on *PTEN*-intact breast cancer cells (Extended Data Fig. 7g, h). One caveat is the potential role of CHD1 as a key oncogenic driver in some cancer types, regardless of *PTEN* status. In such cancers, one would expect the consistent retention of *CHD1* across genotypes.

Finally, we explored the generality of synthetic essentiality. To that end, we searched *in silico* for additional examples of candidate synthetic-essential genes that might have an obligate role in effecting carcinogenesis and tumour maintenance. Analysis of the prostate cancer TCGA database revealed a number of additional candidates that are rarely deleted but typically show increased expression in the context of alterations to specific tumour-suppressor genes, such as *PTEN*, *TP53*, *SMAD4* and *RB1* (Extended Data Table 3). Previous studies have shown that inhibiting these putative synthetic-essential genes could reduce cell proliferation or lead to tumour regression in prostate cancer and other cancer types, indicating their potential roles in synthetic-lethal interactions with putative tumour suppressors in a given cancer type. Further functional analyses will be needed to verify the synthetic essentiality of these genes in cancer cells that harbour specific tumour-suppressor deficiencies, as well as to identify potential regulatory interactions and cell-essential mechanisms.

Although most synthetic-lethal interactions involve two genes in parallel pathways that converge on the same essential biological process (for example, the convergence of BRCA and PARP on DNA-repair processes), the PTEN–CHD1 example indicates that the synthetic-essential gene can serve as an essential downstream effector for a specific deficiency in a tumour-suppressor gene. Our results provide a framework for the discovery of targetable vulnerabilities in cancers harbouring specific tumour-suppressor deficiencies.

Online Content Methods, along with any additional Extended Data display items and Source Data, are available in the online version of the paper; references unique to these sections appear only in the online paper.

Received 26 July; accepted 23 December 2016.
Published online 6 February 2017.

1. Hartwell, L. H., Szankasi, P., Roberts, C. J., Murray, A. W. & Friend, S. H. Integrating genetic approaches into the discovery of anticancer drugs. *Science* **278,** 1064–1068 (1997).
2. Farmer, H. *et al.* Targeting the DNA repair defect in *BRCA* mutant cells as a therapeutic strategy. *Nature* **434,** 917–921 (2005).
3. Muller, F. L. *et al.* Passenger deletions generate therapeutic vulnerabilities in cancer. *Nature* **488,** 337–342 (2012).
4. Cairns, P. *et al.* Frequent inactivation of *PTEN/MMAC1* in primary prostate cancer. *Cancer Res.* **57,** 4997–5000 (1997).
5. Wang, S. *et al.* Prostate-specific deletion of the murine Pten tumor suppressor gene leads to metastatic prostate cancer. *Cancer Cell* **4,** 209–221 (2003).
6. Fece de la Cruz, F., Gapp, B. V. & Nijman, S. M. Synthetic lethal vulnerabilities of cancer. *Annu. Rev. Pharmacol. Toxicol.* **55,** 513–531 (2015).
7. Bryant, H. E. *et al.* Specific killing of BRCA2-deficient tumours with inhibitors of poly(ADP-ribose) polymerase. *Nature* **434,** 913–917 (2005).
8. Nijhawan, D. *et al.* Cancer vulnerabilities unveiled by genomic loss. *Cell* **150,** 842–854 (2012).
9. Thomas, R. K. *et al.* High-throughput oncogene mutation profiling in human cancer. *Nat. Genet.* **39,** 347–351 (2007).
10. Ciriello, G., Cerami, E., Sander, C. & Schultz, N. Mutual exclusivity analysis identifies oncogenic network modules. *Genome Res.* **22,** 398–406 (2012).
11. Mendes-Pereira, A. M. *et al.* Synthetic lethal targeting of PTEN mutant cells with PARP inhibitors. *EMBO Mol. Med.* **1,** 315–322 (2009).
12. Dillon, L. M. & Miller, T. W. Therapeutic targeting of cancers with loss of PTEN function. *Curr. Drug Targets* **15,** 65–79 (2014).
13. Mason, J. M. *et al.* Functional characterization of CFI-400945, a Polo-like kinase 4 inhibitor, as a potential anticancer agent. *Cancer Cell* **26,** 163–176 (2014).
14. Huang, S. *et al.* Recurrent deletion of CHD1 in prostate cancer with relevance to cell invasiveness. *Oncogene* **31,** 4164–4170 (2012).
15. Burkhardt, L. *et al.* CHD1 is a 5q21 tumor suppressor required for ERG rearrangement in prostate cancer. *Cancer Res.* **73,** 2795–2805 (2013).
16. Cancer Genome Atlas Research Network. The molecular taxonomy of primary prostate cancer. *Cell* **163,** 1011–1025 (2015).
17. Rodrigues, L. U. *et al.* Coordinate loss of MAP3K7 and CHD1 promotes aggressive prostate cancer. *Cancer Res.* **75,** 1021–1034 (2015).
18. Hart, M. *et al.* The F-box protein β-TrCP associates with phosphorylated β-catenin and regulates its activity in the cell. *Curr. Biol.* **9,** 207–210 (1999).
19. Zhao, B., Li, L., Tumaneng, K., Wang, C. Y. & Guan, K. L. A coordinated phosphorylation by Lats and CK1 regulates YAP stability through SCF(β-TRCP). *Genes Dev.* **24,** 72–85 (2010).
20. Strack, P. *et al.* SCF(β-TRCP) and phosphorylation dependent ubiquitination of IκBα catalyzed by Ubc3 and Ubc4. *Oncogene* **19,** 3529–3536 (2000).
21. Fuchs, S. Y., Spiegelman, V. S. & Kumar, K. G. The many faces of β-TrCP E3 ubiquitin ligases: reflections in the magic mirror of cancer. *Oncogene* **23,** 2028–2036 (2004).
22. Flanagan, J. F. *et al.* Double chromodomains cooperate to recognize the methylated histone H3 tail. *Nature* **438,** 1181–1185 (2005).
23. Gaspar-Maia, A. *et al.* Chd1 regulates open chromatin and pluripotency of embryonic stem cells. *Nature* **460,** 863–868 (2009).
24. Ben-Neriah, Y. & Karin, M. Inflammation meets cancer, with NF-κB as the matchmaker. *Nat. Immunol.* **12,** 715–723 (2011).
25. Huang, S., Pettaway, C. A., Uehara, H., Bucana, C. D. & Fidler, I. J. Blockade of NF-κB activity in human prostate cancer cells is associated with suppression of angiogenesis, invasion, and metastasis. *Oncogene* **20,** 4188–4197 (2001).
26. Jin, R. *et al.* Inhibition of NF-κB signaling restores responsiveness of castrate-resistant prostate cancer cells to anti-androgen treatment by decreasing androgen receptor-variant expression. *Oncogene* **34,** 3700–3710 (2015).

Supplementary Information is available in the online version of the paper.

Acknowledgements We thank S. W. Hayward for the BPH1 cell line; P. Shepherd for the PDX models, Y. Chen for Flag-tagged β-TrCP plasmid; T. Gutschner for CRISPR X330-Cherry vector; Y. L. Deribe for the HA-tagged PTEN plasmid; S. Jiang and K. Zhao for assistance in maintenance of mouse colonies; Q. E. Chang for assistance in IHC slides scanning; and the MD Anderson Sequencing and Microarray Facility (SMF) and Flow Cytometry and Cellular Imaging Core Facility. This work was supported in part by the Odyssey Program and Theodore N. Law Endowment For Scientific Achievement at The University of Texas MDACC 600649-80-116647-21 (D.Z.); DOD Prostate Cancer Research Program (PCRP) Idea Development Award–New Investigator Option W81XWH-14-1-0576 (X. Lu); NIH Pathway to Independence (PI) Award (K99/R00)-NCI: 1K99CA194289 (G.W.); DOD PCRP W81XWH-14-1-0429 (P.Dey.); CPRIT research training award RP140106-DC (D.C.); NIH grants P01 CA117969 (R.A.D.) and R01 CA084628 (R.A.D.).

Author Contributions D.Z., Y.A.W. and R.A.D. conceived the original hypothesis of synthetic essentiality. D.Z. designed and performed cell-line-derived xenograft-model and signalling-pathway experiments. X.Lu and X.S. performed the patient-derived xenograft-model experiments and siRNA treatment. G.W. performed microarray and GSEA analyses. Z.L. performed ChIP–seq experiments, and M.T. performed ChIP–seq data analysis. W.L. reviewed and scored human tissue sections. P.T. and W.L. provided the human prostate cancer tissue sections. J.L., J.Z. and J.R.C. performed TCGA data analyses. X.Li., S.S., J.R.C., P.Den. and P.C. provided technical support. N.M.N. provided the PDX model. Y.A.W., X. Lu, G.W., Z.L., D.C. and P.Dey provided intellectual contributions throughout the project. D.Z., Y.A.W., D.J.S. and R.A.D. wrote the paper.

Author Information Reprints and permissions information is available at www.nature.com/reprints. The authors declare no competing financial interests. Readers are welcome to comment on the online version of the paper. Correspondence and requests for materials should be addressed to R.A.D. (rdepinho@mdanderson.org) or Y.A.W. (yalanwang@mdanderson.org).

Reviewer Information *Nature* thanks W. Wei and the other anonymous reviewer(s) for their contribution to the peer review of this work.

METHODS

Cell culture and transfection. The PC-3 prostate cancer cell line was cultured in Ham's F-10 Nutrient Mixture medium with 10% FBS. The prostate cancer cell lines LNCaP, 22Rv1 and benign prostatic hyperplasia epithelial cell line BPH-1 were cultured with Gibco RPMI 1640 medium (RPMI) with 10% FBS. BPH1 was provided by S. W. Hayward. The prostate cancer cell line DU145 was cultured in Eagle's minimum essential medium with 10% FBS. The mouse prostate-cancer-derived cell line PtenSmad4 3132 (*Pten*$^{pc-/-}$*Smad4*$^{pc-/-}$) was generated in 2010 as described previously[27], and cultured in DMEM with 10% FBS. The prostate cancer cell lines RWPE-2 and PtenCaP8 were cultured in DMEM with 10% FBS, 25 μg/ml bovine pituitary extract (BPE), 5 μg/ml bovine insulin and 6 ng/ml human recombinant EGF. The breast cancer cell lines BT-549 and MDA-MB-468 were cultured with RPMI with 10% FBS; and the breast cancer cell line T47D was cultured with RPMI with 10% FBS and 5 μg/ml bovine insulin. MDA-MB-231 and 293T cells were cultured in DMEM with 10% FBS. All cell lines were purchased from ATCC, confirmed to be mycoplasma-free, and maintained at 37 °C and 5% CO_2. All human cell lines have been validated through fingerprinting by the MD Anderson Cell Line Core Facility.

All transient transfections of plasmids and siRNA into cell lines followed the standard protocol for Lipofectamine 2000 Transfection Reagent (Thermo Fisher, #11668019). Two siRNA oligos targeting β-TrCP were purchased from Sigma-Aldrich (SASI_Hs01_00189438 and 00189439).

shRNA knockdown of *CHD1*. We screened seven hairpins targeting human *CHD1* transcripts and found two independent sequences that reduced protein levels by >70%. These hairpins were in the pLKO.1 vector (*shCHD1* #2 and #4). The following *CHD1* shRNA sequences were used: *shCHD1* #2: NM_001270.2: 5′-CCGGGCGGTTTATCAAGAGCTATAACTCGAGTTATAGCTCTTGATAAACCGCTTTTT-3′; *shCHD1* #4: NM_001270.2: 5′-CCGGGCGCAGTAGAAGTAGGAGATACTCGAGTATCTCCTACTTCTACTGCGCTTTTT-3′.

In addition, we screened five hairpins targeting mouse *Chd1* and identified two that reduced protein levels by >60%. These hairpins were in the pLKO.1 vector (*shChd1* #1 and #2). The following mouse *Chd1* shRNA sequences were used. *shChd1* #1: NM_007690: 5′-CCGGTCCGAGCACACACATCATAAACTCGAGTTTATGATGTGTGTGCTCGGATTTTTG-3′; *shChd1* #2: NM_007690: 5′-CCGGGCCAGGAGACATACAGTATTTCTCGAGAAATACTGTATGTCTCCTGGCTTTTTG-3′.

Recombinant lentiviral particles were produced by transient transfection of 293T cells. In brief, 8 μg of the shRNA plasmid, 4 μg of the psPAX2 plasmid, and 2 μg of the pMD2.G plasmid were transfected using Lipofectamine 2000 into 293T cells plated in 100-mm dishes. Viral supernatant was collected 48 h and 72 h after transfection and filtered. Cells were infected twice in 48 h with viral supernatant containing 10 μg/ml polybrene, and then selected using 2 μg/ml puromycin and tested for CHD1 expression by immunoblot.

Knockout using CRISPR. Short guide RNAs (sgRNAs) targeting human CHD1 were designed using the Broad Institute sgRNA Designer (http://www.broadinstitute.org/rnai/public/analysis-tools/sgrna-design) and cloned into pX330-Cherry vector individually. The *CHD1* sgRNA sequences are as follows:

*sgCHD1_*#1F: 5′-CACCGGACGCATCATCAGACCAAA-3′; *sgCHD1_*#3F: 5′-CACCGTCAGCTCCATCAACTTTCGG-3′.

The plasmids with sgRNA were transiently transfected into cells using Lipofectamine 2000. Cells were harvested 72 h later, and ten Cherry-positive cells were sorted into each well of a 96-well plate by flow cytometry, followed by immunoblotting for CHD1 protein. PCR sequencing was also performed using genomic DNA extracted from *CHD1*-deficient single clones to identify genetic alteration at the *CHD1* allele. Finally, we chose the single clone in which one or more premature stop codons were introduced in coding exons by sgRNA-induced mutations. An sgRNA plasmid targeting human PTEN was purchased from Santa Cruz Biotechnology (sc-400103); a similar process was performed to generate the *PTEN*-knockout DU145 cell line.

The re-expression of PTEN in *PTEN*-deficient cancer cells provoked proliferative arrest and apoptosis, given that PTEN regulates many hallmarks of cancer.

Cell proliferation assays and apoptosis analysis. Cell proliferation was assayed either through colony formation or cell number counting. For the colony formation assay, 5×10^3 or 1×10^4 cells were seeded in each well of 6-well plates and cultured for 5–7 days. At the end point, cells were fixed and stained with 0.5% crystal violet in 25% methanol for 1 h. For cell number counting, 5×10^3 cells were seeded in each well of 6-well plates for each time point. At the indicated time points, cells were counted using a Countess II FL automated cell counter (Invitrogen). For apoptosis analysis, cells were stained with annexin V PE and DAPI, and evaluated by flow cytometry according to the manufacturer's protocol (Biovision).

Xenograft prostate or breast cancer model. The *in vivo* tumour growth of human prostate or breast cancer cells transduced with a non-targeting hairpin or *shCHD1* was determined using a subcutaneous transplant xenograft model. Cancer cells (2×10^6) in PBS/matrigel mixture were injected subcutaneously into 5-week-old male nude mice (Taconic) or NOD/SCID (non-obese diabetic/severe combined immunodeficient) mice (Charles River) under deep anaesthesia. The resulting tumours were measured twice a week. Once the largest tumour diameter reached the maximal tumour diameter allowed under our institutional protocol, all mice were killed and tumours were collected and weighed. For the PDX model, a *PTEN*-deficient PDX line (MDA-prostate cancer-183, generated by N. M. Navone[28]) was selected from seven candidates by detecting PTEN expression and pAKT levels in tumour lysate by immunoblot. Patient-derived tumour fragments (3–4 mm^3) were surgically xenografted under the skin of male SCID mice. When tumours reached approximately 100 mm^3, mice were assigned randomly into one of two treatment groups. Each tumour was treated weekly (three times total) with 12 μg control siRNA or siRNA targeting *CHD1* using MaxSuppressor *In Vivo* RNALANCEr II (Bio Scientific, #3410-01), following the manufacturer's protocol. Tumour volume was measured before the first treatment (start point) and 3 days after the third treatment (end point). Both negative siRNA control (#VC30002) and human *CHD1* siRNA (SASI_Hs02_00331472; 00203194; 00203195) were purified by high-performance liquid chromatography and purchased from Sigma-Aldrich. All mouse experiments were performed with the approval of the MD Anderson Institutional Animal Care and Use Committee (IACUC) under protocol number 1069. The maximal tumour diameter allowed by the IACUC is 1.5 cm.

Immunoprecipitation and immunoblot. For CHD1 immunoprecipitation, cells were lysed in NP-40 buffer containing 50 mM Tris-HCl (pH 7.5), 150 mM NaCl, 0.3% Nonidet P-40, and protease inhibitor cocktail (Sigma-Aldrich). Cell lysates (500 μl) were incubated with anti-CHD1 antibody (Cell Signaling #4351S) or control IgG overnight at 4 °C. Magnetic or agarose beads (10 μl, Novex, # 10003D) were added to each sample. After 3 h, the beads were washed three times with NP-40 buffer, followed by immunoblotting. For V5-immunoprecipitation, cell lysates were incubated with anti-V5-tag mAb-magnetic beads (MBL International, #M167-9) for 3 h at 4 °C. For the ubiquitination assay, 48 h after transfection, cells were lysed in 1% SDS buffer (50 mM Tris-HCl pH 7.5, 0.5 mM EDTA, 1 mM DTT) and boiled for 15 min, followed by a fivefold dilution in 50 mM Tris-HCl immunoprecipitation buffer. Proteins were blotted following standard protocol. Antibodies specific for CHD1 (Cell Signaling, #4351S), PTEN (Cell Signaling, #9188S), S473P-AKT (Cell Signaling, #3787S), β-TrCP (Cell Signaling, #4394S), H3K4me3 (Cell Signaling, #9751S), Flag (Sigma, #F7425), HA (Santa Cruz, #sc-7392), GSK3β (Cell Signaling, #12456P), and β-actin (Sigma, #A3854) were purchased from the indicated companies. Phos-tag SDS–PAGE (Wako Chemicals, SuperSep Phos-tag, #192-17401) was used to detect phosphorylation of CHD1 following the standard protocol.

Immunohistochemistry and immunofluorescence. Eighty cases of human prostate hyperplasia and cancer samples were purchased from US Biomax (PR807b) and the rest of the samples were acquired from the Prostate Tissue Bank of MD Anderson Cancer Center (total $n = 127$). Immunohistochemistry was performed as previously described[27]. A pressure cooker (95 °C for 30 min followed by 120 °C for 10 s) was used for antigen retrieval using Antigen Unmarking Solution (Vector Laboratories). Antibodies specific to CHD1 (Sigma, #HPA022236) and PTEN (Cell Signaling, #9188S) were purchased. The human tissue sections were reviewed and scored in a blinded manner for staining intensity (0–2) by W.L. High expression of CHD1 corresponded to a staining score of 2, whereas low expression corresponded to staining scores 0 and 1. Slides were scanned using Pannoramic 250 Flash III (3DHISTECH Ltd) and images were captured through Pannoramic Viewer software (3DHISTECH Ltd). Procedures related to human specimens were approved by the MD Anderson Institutional Review Board under protocol number #PA14-0420; human samples from MD Anderson tissue banks were obtained with the informed consent from the patients for tissue collection for research purposes.

PC-3 cells were infected with GFP–PTEN lentiviral particles for 72 h, fixed and stained using anti-CHD1 antibodies (Sigma, #HPA022236) following the standard protocol. Images were captured using a fluorescence microscope (Leica DMi8).

Migration assay. Prostate cancer cells (1×10^4) were suspended in serum-free culture medium and seeded into 24-well Transwell inserts (8.0 μm). Medium with serum was added to the remaining receiver wells. After 24 h, the inside of each insert was gently swabbed, and crystal violet solution was added for 1 h for staining.

ChIP–seq. ChIP was performed as described[29]. Briefly, chromatin from formaldehyde-fixed cells (control and *CHD1*-knockdown PC-3 cells, 1×10^7 cells for anti-CHD1 antibody and 1×10^6 cells for anti-H3K4me3 antibody) were cross-linked using 1% paraformaldehyde for 10 min and reactions were quenched by addition of 0.125 M glycine for 5 min at room temperature. Cells were lysed with ChIP lysis buffer (10 mM Tris-HCl (pH 8.0), 1 mM EDTA (pH 8.0), 140 mM NaCl, 1% Triton X-100, 0.2% SDS, 0.1% deoxycholic acid) for 30 min on ice. Chromatin fragmentation was performed using a Diagenode BioruptorPico sonicator (30 s on, 30 s off for 45 cycles) to achieve a DNA shear length of 200–500 bp. Solubilized chromatin

was then incubated overnight with the appropriate antibody–Dynabead (Life Technologies) mixture (anti-CHD1 antibody: Bethyl, #A301-218A; anti-H3K4me3 antibody: Abcam, #ab8580). Immune complexes were then washed three times with RIPA buffer, once with RIPA-500 (RIPA with 500 mM NaCl), and once with LiCl wash buffer (10 mM Tris-HCl (pH 8.0), 1 mM EDTA (pH 8.0), 250 mM LiCl, 0.5% NP-40, 0.5% deoxycholic acid). Elution and reverse-crosslinking were performed in direct elution buffer (10 mM Tris-Cl (pH 8.0), 5 mM EDTA, 300 mM NaCl, 0.5% SDS) with proteinase K (20 mg/ml) at 65 °C overnight. Eluted DNA was purified using AMPure beads (Beckman-Coulter). Libraries were prepared using NEBNext Ultra DNA Library kit (E7370). Sequencing was performed using an Illumina HiSeq 2500 instrument to generate dataset GSE91401. Reads were aligned to a reference genome (UCSC hg19; http://hgdownload.cse.ucsc.edu/downloads.html#human) using the Burrows–Wheeler Aligner. Reads mapping to more than two genomic loci were ignored.

mRNA expression analysis and microarray. Cells were lysed in TRIzol Reagent (Invitrogen; #15596-026), followed by total RNA isolation using the standard protocol. The RNA was further purified using RNeasy (QIAGEN) according to the manufacturer's protocol and reverse-transcribed into cDNA using the SuperScript III First-Strand Synthesis System (Invitrogen). qPCR was performed for target-gene-expression analysis using the SYBR Green PCR Master Mix (Applied Biosystems); indicated primers are listed in Supplementary Table 5. Microarray analysis was performed on RNA prepared from control and *CHD1*-knockdown PC-3 or *CHD1*-knockout LNCaP cells (biological triplicates for control and each *CHD1* shRNA or *CHD1*-knockout) at the MD Anderson Microarray Core facility using the GeneChip Human Genome U133 Plus 2.0 Array (Affymetrix) to generate dataset GSE84970. Genes that were differentially expressed between control and *CHD1*-depleted groups were subjected to ingenuity pathway analysis (IPA) and gene set enrichment analysis (GSEA). The GSE25140 dataset, published in 2011, of wild-type and *Pten* deletion mouse prostate tissues was downloaded from the NCBI GEO database repository[27]. The raw data were processed and analysed by GenePattern using Expression File Creator Module (version 12.3) and GSEA module (v17). The default GSEA basic parameters were used and a *t*-test was used as the metric for ranking genes.

Computational analysis of human prostate TCGA data. A list of 60 downregulated genes (fold change >2) in the TNF–NF-κB pathway identified by microarray analysis was generated (Extended Data Table 2). The mRNA expression *z* scores of each gene in 498 TCGA prostate cancer samples were downloaded from http://www.cbioportal.org. The two-tailed Pearson correlations between CHD1 expression and indicated genes were calculated using SPSS Statistics software (IBM), and *P* values were determined by two-tailed Fisher's exact test. The gene list was then ranked by Pearson's correlation with CHD1 expression. The heat map was generated using Microsoft Excel Graded Colour Scale function with a three-colour scale set at numbers −1, 0, and 1. For the analysis of mutual exclusiveness and gene expression listed in Extended Data Table 3, the genetic alteration and gene expression of 332 TCGA prostate cancer samples with mRNA, copy number alterations and sequencing data were downloaded from http://gdac.broadinstitute.org/runs/stddata__2016_01_28/data/PRAD/20160128/ and analysed. The odds ratio score was calculated to indicate mutual exclusiveness between gene *A* and gene *B* deletion. The mean values of gene *B* expression in all 332 samples and that in gene *A* deleted samples were calculated, and *P* values were determined by two-tailed student *t*-test.

Statistics. Images of genomic alterations in TCGA database were captured from http://www.cbioportal.org. Estimations of sample size were done taking into consideration previous experience with animal strains, assay sensitivity and tissue collection methodology used. The two-tailed Pearson correlation between CHD1 and PTEN expression or Gleason grades was calculated using SPSS Statistics software (IBM), and *P* values were determined by two-tailed Fisher's exact test. The Student *t*-test assuming two-tailed distributions was used to calculate statistical significance between groups (GraphPad Prism 6 or Microsoft Excel). The *n* value represents biological replicates. Error bars indicate standard deviation (s.d.). The *P* values shown in the tumour growth plot (Fig. 1 and Extended Data Figs 2, 3, 7) indicate the differences in tumour sizes at the end-point. For IPA, we included all 50 'hallmark' gene sets of the Molecular Signatures Database (MSigDB) as described[30] as customized pathways. Then a list of downregulated genes in *CHD1*-knockdown PC-3 cells generated from microarray (Supplementary Table 3) or the peak-score list generated from ChIP (Supplementary Table 1 or 2) was uploaded for IPA core analysis. The filter threshold of microarray data was a fold change (control versus *shCHD1*) >1.5.

Data availability. The Microarray dataset generated during the current study has been deposited in the Gene Expression Omnibus (GEO) repository under accession number GSE84970. The ChIP–seq dataset generated in this study has been deposited in GEO repository under accession number GSE91401. The ChIP–seq signal annotated file and alternatively expressed genes lists (fold change >1.5) generated in this study are included in this published article (and its Supplementary Information). Relevant TCGA datasets were downloaded from http://gdac.broadinstitute.org/runs/stddata__2016_01_28/data/PRAD/20160128/ or http://www.cbioportal.org. All other data are available from the corresponding author upon reasonable request.

27. Ding, Z. *et al.* SMAD4-dependent barrier constrains prostate cancer growth and metastatic progression. *Nature* **470,** 269–273 (2011).
28. Wan, X. *et al.* Prostate cancer cell-stromal cell crosstalk via FGFR1 mediates antitumor activity of dovitinib in bone metastases. *Sci. Transl. Med.* **6,** 252ra122 (2014).
29. Garber, M. *et al.* A high-throughput chromatin immunoprecipitation approach reveals principles of dynamic gene regulation in mammals. *Mol. Cell* **47,** 810–822 (2012).
30. Liberzon, A. *et al.* The Molecular Signatures Database (MSigDB) hallmark gene set collection. *Cell Syst.* **1,** 417–425 (2015).

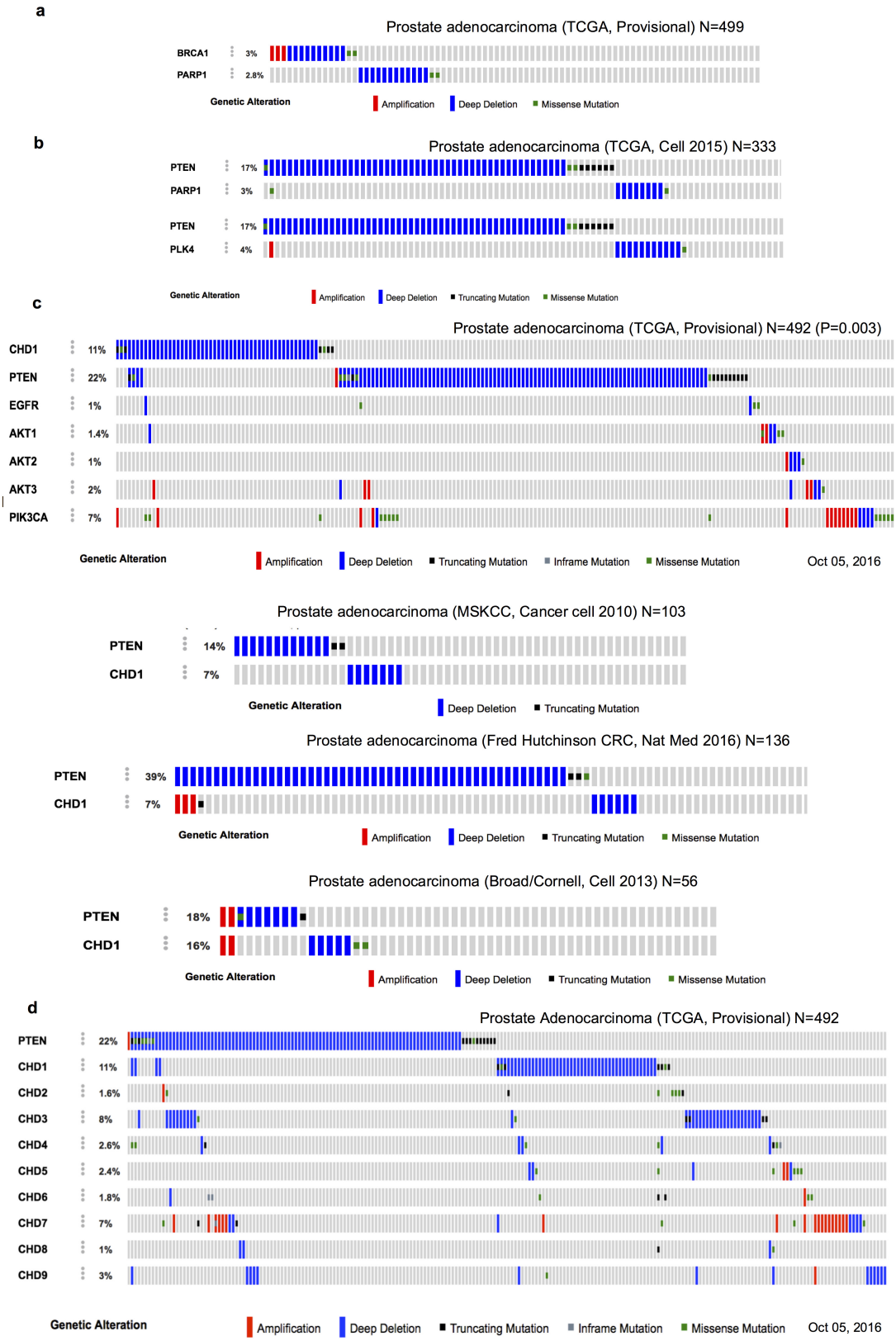

Extended Data Figure 1 | Mutually exclusive deletion patterns in prostate cancer genome. a–d, Genetic alterations of *BRCA1–PARP1* (**a**), *PTEN–PARP1*, and *PTEN–PLK4* (**b**), *CHD1–PTEN* (**c**), and *PTEN–CHD* homologues (**d**) in prostate cancer databases. The gene alteration percentages are shown.

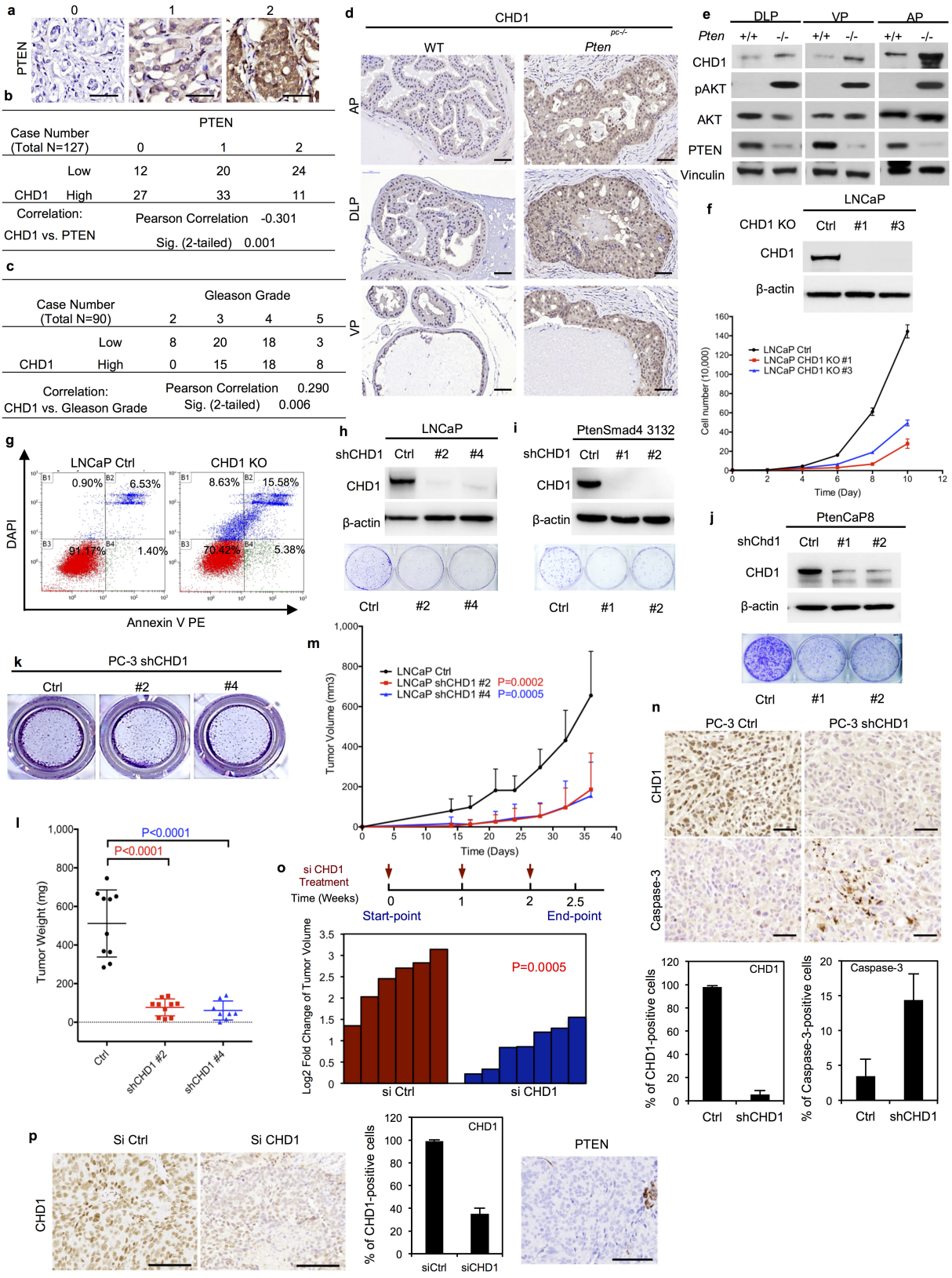

Extended Data Figure 2 | See next page for caption.

Extended Data Figure 2 | Inhibiting CHD1 suppresses tumour growth of PTEN-null prostate cancer. a, Representative images of PTEN staining (scores 0–2). **b**, The negative correlation between CHD1 and PTEN staining in human prostate cancer samples was analysed by two-tailed Pearson's correlation coefficient. **c**, The correlation between CHD1 staining and Gleason grade in human prostate cancer samples was analysed by two-tailed Pearson correlation coefficient. **d**, **e**, Representative CHD1 staining and immunoblots of lysates of prostate tissues of wild-type and prostate-specific *Pten*-deleted mice ($Pten^{pc-/-}$). AP, anterior prostate; DLP, dorsal lateral prostate; VP, ventral prostate. pAKT indicates phosphorylation of AKT at Ser473. **f**, Immunoblots of lysates generated from *CHD1*-knockout and control LNCaP cells. Cell proliferation was determined by counting cell numbers in triplicate wells. **g**, *CHD1*-knockout and control LNCaP cells were stained with annexin V, phycoerythrin (PE) and DAPI; cell apoptosis was detected by flow cytometry. **h**–**j**, Immunoblots of lysates and colony formation assays generated from *CHD1*-knockdown and control LNCaP cells, PtenSmad4 3132 cells (a mouse prostate cancer cell line generated from the *Pten Smad4* co-deletion prostate cancer mouse model) or PtenCap8 cells (a mouse prostate cancer cell line generated from the *Pten*-deletion prostate cancer mouse model). **k**, Representative migration images of *CHD1*-knockdown and control PC-3 cells determined by transwell assay. **l**, Weight of subcutaneous tumours derived from *CHD1*-knockdown and control PC-3 cells ($n = 10$ for both control and *shCHD1* #2 groups; $n = 8$ for *shCHD1* #4 group). **m**, Growth of subcutaneous tumours derived from *CHD1*-knockdown and control LNCaP cells ($n = 10$ for both control and *shCHD1* #2 groups; $n = 8$ for *shCHD1* #4 group). **n**, Representative images and quantification of CHD1 and caspase-3 staining in subcutaneous tumour tissues generated by *CHD1*-knockdown and control PC-3 cells ($n = 4$). **o**, Mice bearing patient-derived xenografts (PDX) were treated with siRNA targeting *CHD1* at three time points (40 μg per tumour per week). Fold changes of tumour volume are shown (siCtrl group $n = 6$; *siCHD1* group $n = 7$). **p**, Representative images and quantification of CHD1-stained xenograft tumour tissues generated in **o** ($n = 4$). *PTEN* status of the PDX tumour. Error bars indicate s.d. (**f**, **l**, **m**, **n**, **p**), *P* values were determined by two-tailed *t*-test. Scale bars, 50 μm (**a**, **d**, **n**), 100 μm (**p**). Representative data of triplicate experiments are shown.

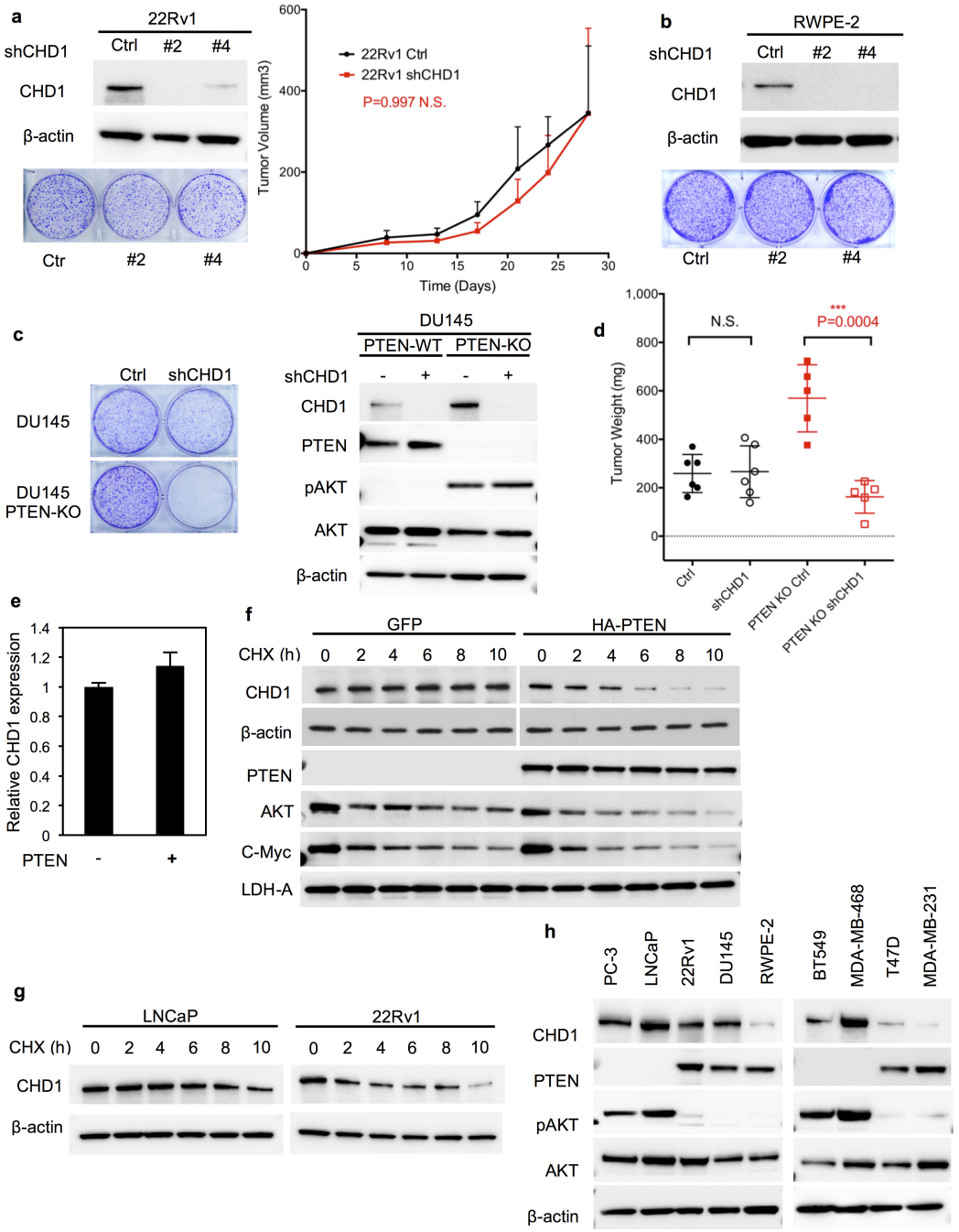

Extended Data Figure 3 | Targeting CHD1 has minimal impact on tumour growth of PTEN-intact prostate cancer. a, Immunoblots of lysates and colony-formation assays generated from *CHD1*-knockdown and control 22Rv1 cells, followed by measurement of subcutaneous tumour growth *in vivo* (control group $n = 8$; *shCHD1* group $n = 7$). **b**, Immunoblots of lysates and colony formation assays generated from *CHD1*-knockdown and control RWPE-2 cells. **c**, Immunoblots of lysates and colony formation assays generated from *CHD1*-knockdown wild-type or *PTEN*-knockout DU145 cells. **d**, Weights of subcutaneous tumours derived from *CHD1*-knockdown DU145 cells ($n = 5$ for the *PTEN*-knockout *shCHD1* group; other group $n = 6$). **e**, *CHD1* mRNA levels were detected by qPCR in PC-3 cells overexpressing PTEN. **f**, Immunoblot time courses of CHD1 protein in control PC-3 (GFP) and PTEN-overexpressing (HA–PTEN) cells treated with 50 μg ml^{-1} cycloheximide (CHX). C-Myc was used as the positive control, LDH-A as the negative control. **g**, Immunoblot time courses of CHD1 protein in LNCaP and 22Rv1 cells treated with cycloheximide. **h**, Immunoblot of CHD1 protein in PTEN-intact and -deficient cell lines. Error bars in **a** and **d** indicate s.d. *P* values were determined by two-tailed *t*-test. N.S., not significant.

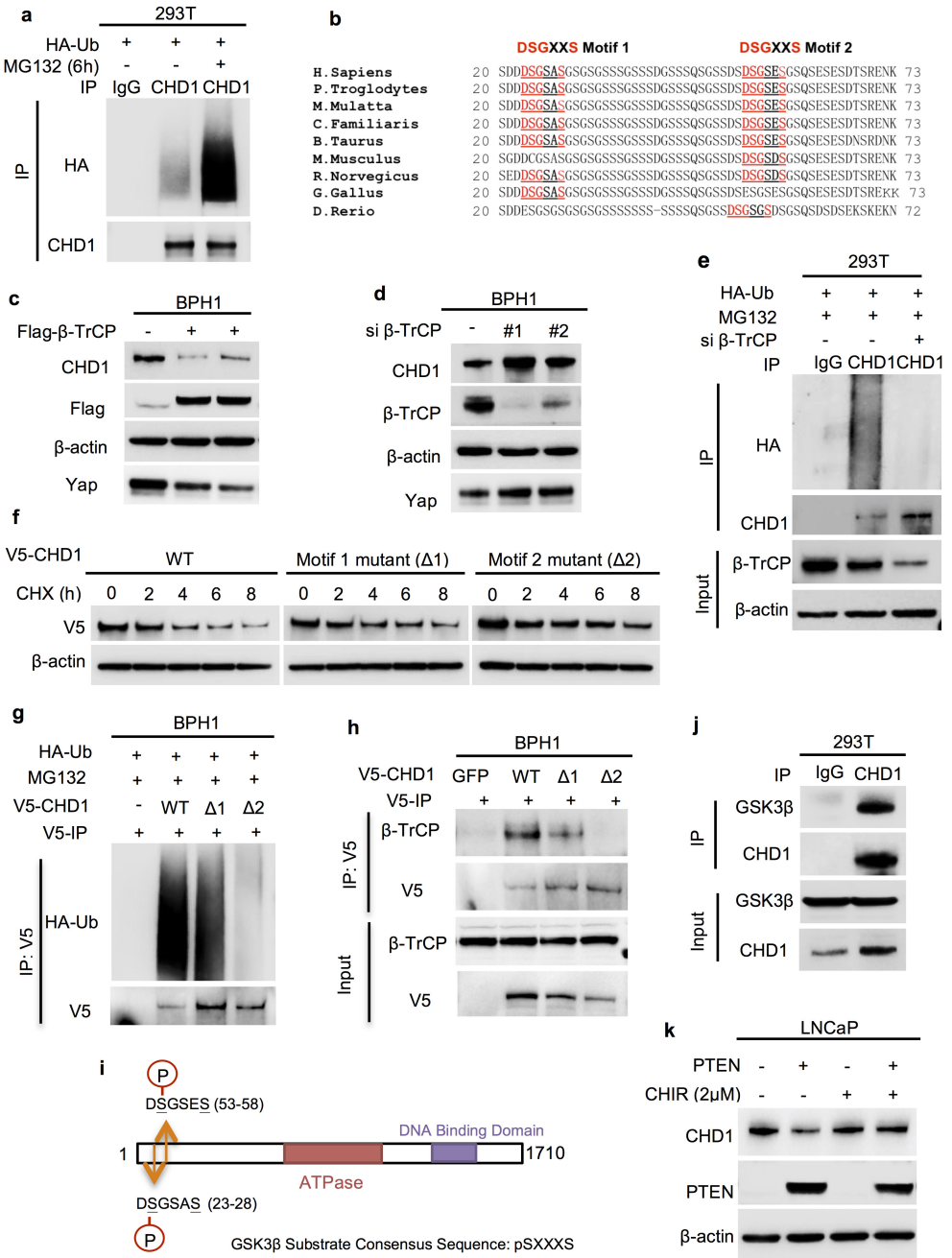

Extended Data Figure 4 | PTEN–AKT–GSK3β pathway promotes CHD1 degradation through β-TrCP-mediated ubiquitination–proteasome pathway. a, HA-tagged ubiquitin (HA–Ub) was transfected into 293T cells for 40 h, followed by 6 h of MG132 treatment and immunoprecipitation (IP) of endogenous CHD1. CHD1 and HA were detected by immunoblot. **b**, Conservation of two β-TrCP binding motifs in vertebrates. **c**, **d**, Immunoblots of CHD1 in BPH1 cells overexpressing Flag-tagged β-TrCP or knockdown of β-TrCP (Yap as positive control). **e**, HA–Ub and *siBTRC* (targeting β-TrCP) were transfected into 293T cells for 48 h, followed by 8-h of treatment with MG132 treatment (10 μM) and detection of ubiquitin-bound CHD1 by immunoblot. **f**, V5-tagged wild-type (WT) or two β-TrCP binding motif mutants (DSGXXS ≥ DAGXXA) of CHD1 were introduced into BPH1 cells, followed by CHX treatment over a time course, and V5-tagged CHD1 was detected by immunoblot. **g**, **h**, V5-tagged wild type or the two β-TrCP-binding-motif mutants of CHD1 were introduced into BPH1 cells, followed by V5-immunoprecipitation and detection of ubiquitination and β-TrCP binding by immunoblot. **i**, Schematic diagram of GSK3β substrate consensus sequences in β-TrCP binding motifs of CHD1. **j**, Endogenous CHD1 was immunoprecipitated, followed by immunoblot using GSK3β antibody. **k**, LNCaP cells overexpressing PTEN were treated with 2 μM CHIR for 24 h, and CHD1 protein levels were detected by immunoblot. β-actin was used as a loading control. Representative data of triplicate experiments are shown.

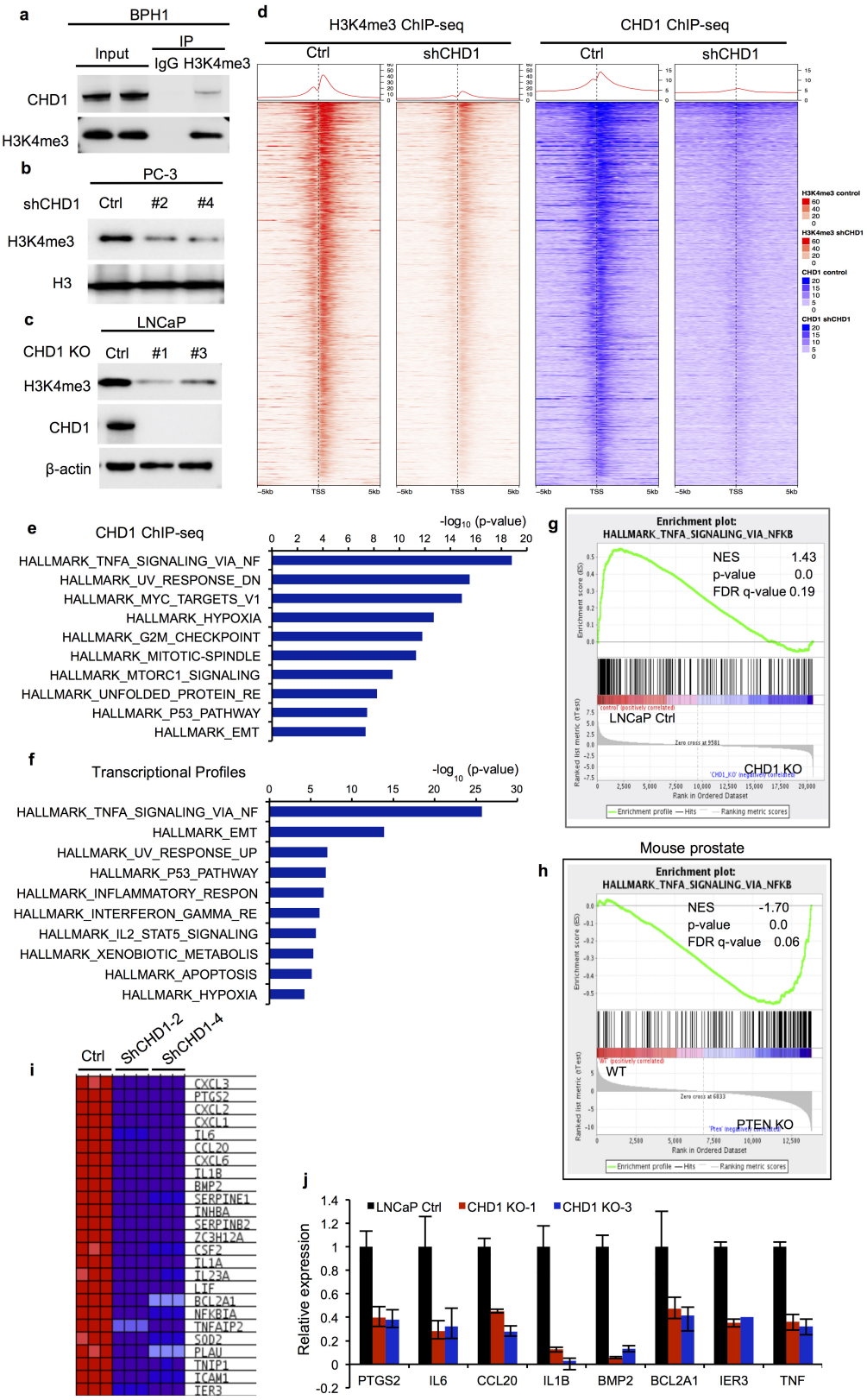

Extended Data Figure 5 | See next page for caption.

Extended Data Figure 5 | CHD1 collaborates with H3K4me3 to activate gene transcription. a, Endogenous H3K4me3 was immunoprecipitated from BPH1 cells and CHD1 binding was detected by immunoblot. **b**, **c**, Immunoblots of H3K4me3 in *CHD1*-knockdown PC-3 cells or *CHD1*-knockout LNCaP cells. **d**, Heat maps showing the CHD1- and H3K4me3-binding features across gene promoters in *shCHD1*-treated versus control shRNA (Ctrl)-treated PC-3 cells (only CHD1/H3K4me3-overlap genes shown). Each panel represents 5 kb upstream and downstream of the transcription start site. **e**, Top ten hallmark pathways showing enrichment of CHD1-target genes identified by ChIP–seq. Fifty MSigDB hallmark pathways emerged following IPA core analysis. Graph displays category scores as $-\log_{10}(P \text{ value})$ from Fisher's exact test. **f**, Microarray analysis was performed in *CHD1*-knockdown and control PC-3 cells. Top ten hallmark pathways exhibiting enrichment of the downregulated genes in *shCHD1* PC-3 cells (fold changes > 1.5). **g**, **h**, GSEA correlation of NF-κB signature with alternatively expressed genes in *CHD1*-knockout LNCaP cells (**g**) and wild-type and *PTEN*-knockout mouse prostate tissues (**h**). Normalized enrichment score (NES), nominal *P*-value and false discovery rate *q* value of correlation are shown. **i**, Heat map representation of 25 most downregulated NF-κB pathway genes in *CHD1*-knockdown PC-3 cells (from blue (low expression) to red (high expression)). **j**, Validation of *CHD1*-regulating genes in two individual *CHD1*-knockout LNCaP cells using qPCR. Data are mean ± s.d. of triplicate experiments.

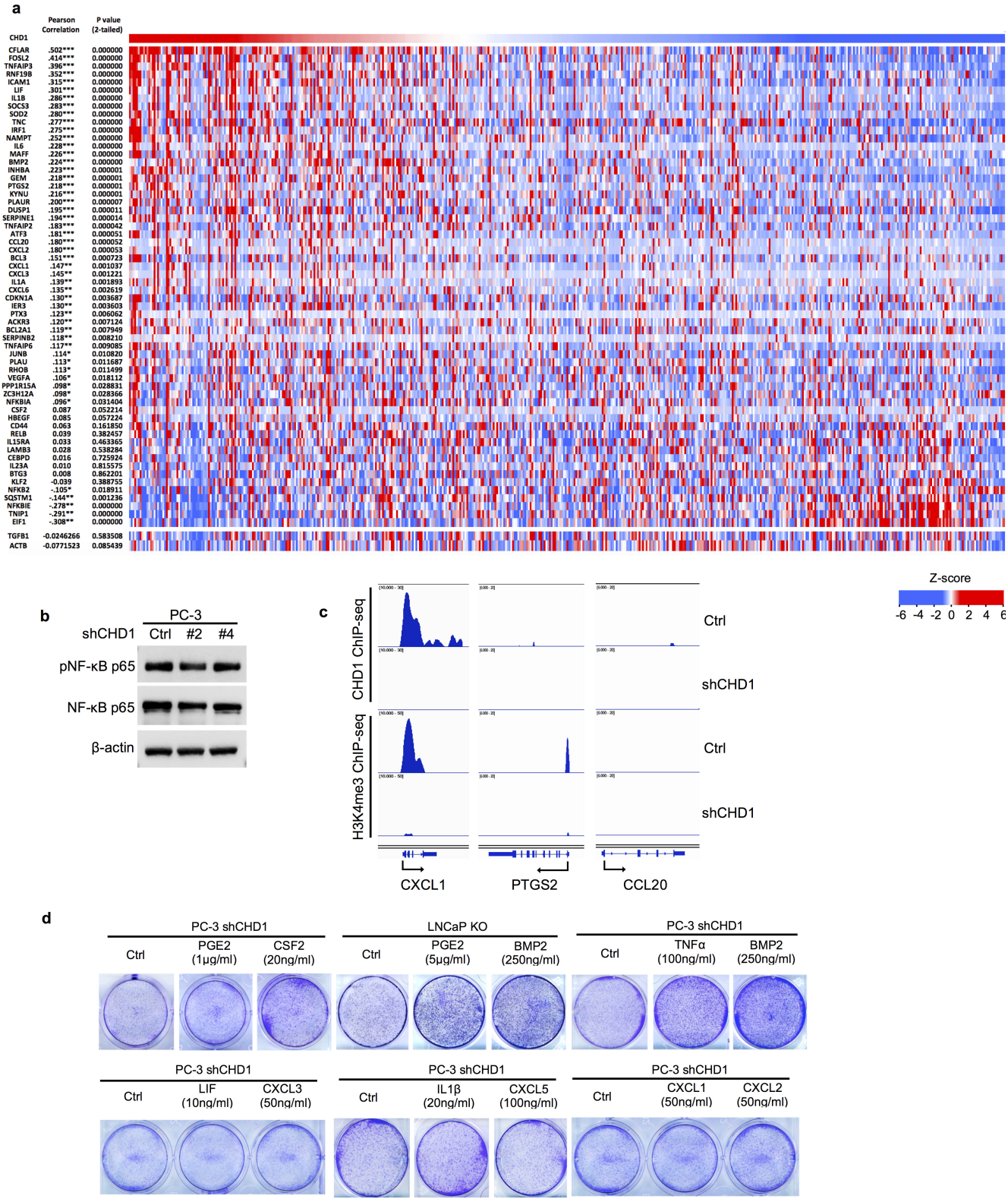

Extended Data Figure 6 | CHD1 activates gene transcription in NF-κB pathway. a, Heat maps showing expression of downregulated TNF–NF-κB pathway genes in 498 TCGA prostate samples, with all samples sorted relative to *CHD1* expression level (shown in top bar). Gene names, Pearson's correlation coefficient between *CHD1* and indicated genes and two-tailed *P* value are shown. **b**, Immunoblot of total and activated NF-κB p65 in control and *CHD1*-knockdown PC-3 cells. **c**, CHD1/H3K4me3-enriched profiles at indicated genes in *CHD1*-knockdown and control PC-3 cells. **d**, Colony-formation assays of *CHD1*-knockdown PC-3 cells rescued by addition of indicated recombinant proteins or PGE2 (prostaglandin E2), the metabolic product of PTGS2.

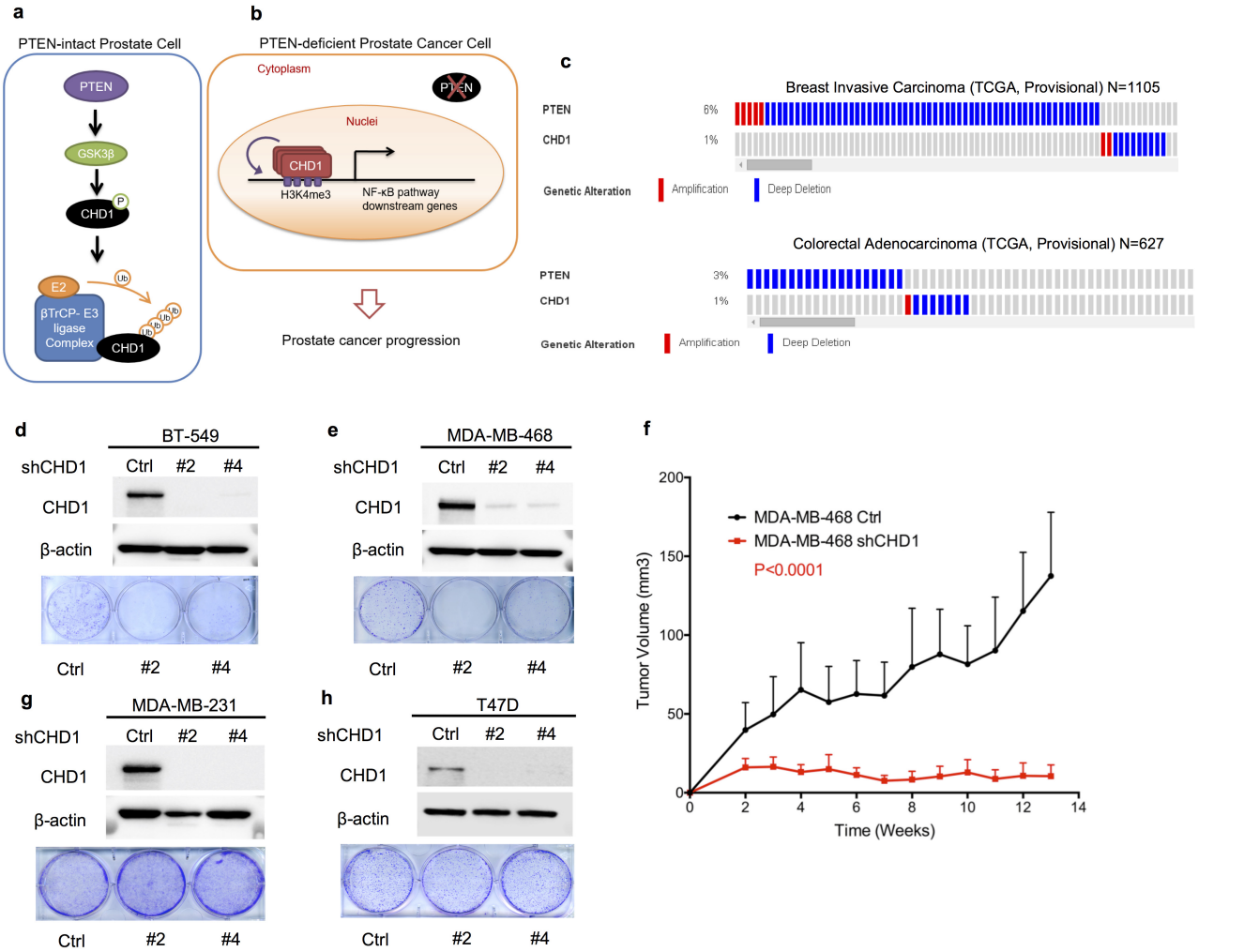

Extended Data Figure 7 | *CHD1* shows synthetic essentiality in *PTEN*-deficient breast cancer. a, **b**, Schematic representations of the role of CHD1 in prostate cancer. In *PTEN*-intact prostate cells, GSK3β is activated by PTEN through inhibition of AKT and phosphorylates CHD1, which stimulates its degradation through the β-TrCP-mediated ubiquitination–proteasome pathway (**a**). However, in *PTEN*-deficient prostate cancer cells, accumulated CHD1 interacts with and maintains H3K4me3, followed by transcriptional activation of genes downstream of NF-κB, leading to disease progression (**b**). **c**, Mutual exclusivity of *PTEN* and *CHD1* deletions also occurs in breast cancer and colon cancer. **d**, **e**, Immunoblots of lysates and colony-formation assays generated from *CHD1*-knockdown and control BT549 and MDA-MB-468 cells. **f**, Growth of subcutaneous tumours derived from *CHD1*-knockdown MDA-MB-468 cells (control group, $n = 10$; *shCHD1* group, $n = 8$). Error bars indicate s.d., *P* values were determined by two-tailed *t*-test. **g**, **h**, Immunoblots of lysates and colony formation assays generated from *CHD1*-knockdown and control MDA-MB-231 and T47D cells. Representative data of triplicate experiments are shown.

Extended Data Table 1 | The 30 most downregulated genes in *CHD1*-knockdown PC-3 cells

	Gene Name	Fold Change (Ctrl/shCHD1)
1	chemokine (C-X-C motif) ligand 5, CXCL5	268.6616213
2	S100 calcium binding protein A8, S100A8	177.2496755
3	lipocalin 2, LCN2	62.23575313
4	**chemokine (C-X-C motif) ligand 3, CXCL3**	**61.23078885**
5	**prostaglandin-endoperoxide synthase 2 (prostaglandin G/H synthase and cyclooxygenase), PTGS2**	**56.11995411**
6	S100 calcium binding protein A9, S100A9	44.14645634
7	**interleukin 8, IL8**	**35.64989451**
8	**chemokine (C-X-C motif) ligand 2, CXCL2**	**31.37390813**
9	**chemokine (C-X-C motif) ligand 1 (melanoma growth stimulating activity, alpha), CXCL1**	**27.15252757**
10	chromosome 8 open reading frame 4, C8orf4	27.09241053
11	brain expressed, X-linked 1, BEX1	25.25263821
12	serpin peptidase inhibitor, clade B (ovalbumin), member 3, SERPINB3	24.09258976
13	**interleukin 6 (interferon, beta 2), IL6**	**20.87206377**
14	complement component 3, C3	20.49050477
15	transforming growth factor, beta-induced, 68kDa, TGFBI	19.19589456
16	**chemokine (C-C motif) ligand 20, CCL20**	**18.37413513**
17	**chemokine (C-X-C motif) ligand 6 (granulocyte chemotactic protein 2), CXCL6**	**18.16844795**
18	cytochrome b5 reductase 2, CYB5R2	17.12023197
19	chromosome 15 open reading frame 48, C15orf48	16.9709983
20	aquaporin 3 (Gill blood group), AQP3	16.50004445
21	**interleukin 1, beta, IL1B**	**15.92818569**
22	hypothetical protein LOC285628, LOC285628	12.89755561
23	prostaglandin E synthase, PTGES	12.81294498
24	pro-platelet basic protein (chemokine (C-X-C motif) ligand 7), PPBP, CXCL7	11.50025421
25	cytochrome P450, family 1, subfamily B, polypeptide 1, CYP1B1	11.36293073
26	NADPH oxidase, EF-hand calcium binding domain 5, NOX5	10.35608831
27	fasciculation and elongation protein zeta 1 (zygin I), FEZ1	10.32840696
28	galanin prepropeptide, GAL	10.22785538
29	**bone morphogenetic protein 2, BMP2**	**10.18134837**
30	interleukin 1 family, member 7 (zeta), IL1F7	10.18103235

The 30 most downregulated genes in *shCHD1*- versus control-treated PC-3 cells are shown. The 10 genes highlighted in bold are known to be downstream genes in the NF-κB pathway.

Extended Data Table 2 | The downregulated NF-κB pathway genes in *CHD1*-knockdown PC-3 cells

Gene Symbol	Entrez Gene Name	Peak Score (ChIP-seq) CHD1	Peak Score (ChIP-seq) H3K4me3	Exp Fold Change (Ctrl/shCHD1)
CXCL3	C-X-C motif chemokine ligand 3	20.8477	28.1396	61.231
CXCL2	C-X-C motif chemokine ligand 2	18.31	24.2217	31.374
CXCL1	C-X-C motif chemokine ligand 1	20.9437	25.1565	27.153
IL6	interleukin 6	12.8091	10.9158	20.872
CXCL6	C-X-C motif chemokine ligand 6	12.5971	22.7408	18.168
IL1B	interleukin 1 beta	17.5558	11.7779	15.928
INHBA	inhibin beta A	19.6438	17.8982	7.954
ZC3H12A	zinc finger CCCH-type containing 12A	15.2155	34.8075	7.19
PLAU	plasminogen activator, urokinase	41.0902	59.2763	4.763
NFKBIA	NFKB inhibitor alpha	26.6431	40.0661	4.473
CD44	CD44 molecule (Indian blood group)	11.8957	24.3992	4.211
FOSL2	FOS like antigen 2	16.331	26.8986	3.349
TNIP1	TNFAIP3 interacting protein 1	15.5569	21.336	3.233
IER3	immediate early response 3	28.1256	26.4733	3.054
ACKR3	atypical chemokine receptor 3	7.70203	8.73691	3.025
DUSP1	dual specificity phosphatase 1	18.9257	25.6815	2.698
NAMPT	nicotinamide phosphoribosyltransferase	12.8093	24.4044	2.627
CFLAR	CASP8 and FADD like apoptosis regulator	14.2285	21.6311	2.544
LAMB3	laminin subunit beta 3	13.0399	18.6755	2.525
CEBPD	CCAAT/enhancer binding protein delta	6.54248	22.0576	2.447
JUNB	jun B proto-oncogene	20.7099	32.9637	2.379
VEGFA	vascular endothelial growth factor A	16.1158	28.7962	2.243
BTG3	BTG family member 3	9.71861	26.8775	2.161
PPP1R15A	protein phosphatase 1 regulatory subunit 15A	10.0349	26.0106	2.136
GEM	GTP binding protein overexpressed in skeletal muscle	10.957	28.2779	2.1
IRF1	interferon regulatory factor 1	12.3429	21.9984	2.096
PTX3	pentraxin 3	17.3919	29.0129	2.052
FJX1	four jointed box 1	19.6547	32.1701	1.847
PHLDA1	pleckstrin homology like domain family A member 1	28.5275	51.8317	1.826
DUSP4	dual specificity phosphatase 4	26.8631	29.1908	1.737
FOSL1	FOS like antigen 1	39.8505	36.7278	1.607
CYR61	cysteine rich angiogenic inducer 61	20.7935	29.9102	1.598
JUN	jun proto-oncogene	19.585	39.506	1.592
SDC4	syndecan 4	12.2208	28.5915	1.553
IER5	immediate early response 5	13.3464	22.5679	1.544
IER2	immediate early response 2	31.4396	49.4192	1.525
ETS2	ETS proto-oncogene 2, transcription factor	13.4695	30.3076	1.505
CEBPB	CCAAT/enhancer binding protein beta	17.7794	0	1.73
PTGS2	prostaglandin-endoperoxide synthase 2	0	10.3651	56.12
BMP2	bone morphogenetic protein 2	0	20.9614	10.181
CSF2	colony stimulating factor 2	0	12.0562	6.422
LIF	leukemia inhibitory factor	0	13.7197	5.375
KYNU	kynureninase	0	10.8662	5.097
TNFAIP2	TNF alpha induced protein 2	0	19.0498	3.92
SOD2	superoxide dismutase 2, mitochondrial	0	20.1497	3.542
ICAM1	intercellular adhesion molecule 1	0	17.779	3.173
CDKN1A	cyclin-dependent kinase inhibitor 1A	0	27.1233	2.94
PLAUR	plasminogen activator, urokinase receptor	0	20.5747	2.872
TNC	tenascin C	0	12.682	2.821
NFKBIE	NFKB inhibitor epsilon	0	22.8154	2.801
HBEGF	heparin binding EGF like growth factor	0	27.7034	2.741
AREG	amphiregulin	0	11.5075	2.663
NFKB2	nuclear factor kappa B subunit 2	0	18.1199	2.593
RELB	RELB proto-oncogene, NF-kB subunit	0	14.7293	2.57
SOCS3	suppressor of cytokine signaling 3	0	44.0616	2.476
BCL3	B-cell CLL/lymphoma 3	0	14.1549	2.388
RNF19B	ring finger protein 19B	0	28.4536	2.361
SQSTM1	sequestosome 1	0	24.3794	2.328
IL15RA	interleukin 15 receptor subunit alpha	0	26.6349	2.324
TNFAIP3	TNF alpha induced protein 3	0	9.96643	2.212
EIF1	eukaryotic translation initiation factor 1	0	19.1981	2.199
KLF2	Kruppel-like factor 2	0	23.576	2.173
MAFF	v-maf avian musculoaponeurotic fibrosarcoma oncogene homolog F	0	26.0075	2.101
ATF3	activating transcription factor 3	0	37.8612	2.081
RHOB	ras homolog family member B	0	32.8819	2.032
TRIP10	thyroid hormone receptor interactor 10	0	37.5187	1.95
GADD45B	growth arrest and DNA damage inducible beta	0	29.8176	1.945
SAT1	spermidine/spermine N1-acetyltransferase 1	0	14.176	1.908
TAP1	transporter 1, ATP-binding cassette, sub-family B (MDR/TAP)	0	28.2344	1.906
PER1	period circadian clock 1	0	17.6631	1.813
SERPINB8	serpin family B member 8	0	22.5062	1.786
TNFSF9	tumor necrosis factor superfamily member 9	0	23.0011	1.762
SPSB1	splA/ryanodine receptor domain and SOCS box containing 1	0	29.9498	1.735
TUBB2A	tubulin beta 2A class IIa	0	26.5246	1.719
SNN	stannin	0	19.8059	1.63
NR4A1	nuclear receptor subfamily 4 group A member 1	0	22.6394	1.626
MARCKS	myristoylated alanine rich protein kinase C substrate	0	15.7629	1.613
EHD1	EH domain containing 1	0	39.3525	1.584
TNIP2	TNFAIP3 interacting protein 2	0	21.4255	1.579
CD83	CD83 molecule	0	26.8444	1.569
BTG2	BTG family member 2	0	36.7798	1.542
CCL20	C-C motif chemokine ligand 20	0	0	18.374
SERPINE1	serpin family E member 1	0	0	9.249
SERPINB2	serpin family B member 2	0	0	7.824
BCL2A1	BCL2 related protein A1	0	0	7.616
TNFAIP6	TNF alpha induced protein 6	0	0	7.377
IL1A	interleukin 1 alpha	0	0	6.351
IL23A	interleukin 23 subunit alpha	0	0	5.887
PLPP3	phospholipid phosphatase 3	0	0	1.607
B4GALT1	beta-1,4-galactosyltransferase 1	0	0	1.503

A summary of 90 downregulated NF-κB pathway genes in *CHD1*-knockdown PC-3 cells, including expression fold changes and the peak scores of binding sites with CHD1 or enrichment of the H3K4me3 modification.

Extended Data Table 3 | Mutual exclusiveness pairs in prostate cancer

Gene A	Gene B	#Deletion (#Total samples=332)			Mutual Exclusiveness score*	Gene B Expression		P-VALUE	Gene B Description	Function in cancer
		Only in A	Only in B	In A and B		Mean In A Del samples	Mean in all samples			
PTEN (Deletion)	PARP1	64	7	1	-0.784987109	4104.537726	3716.751276	0.000887378	Poly [ADP-ribose] polymerase 1	PARP1 has a role in repair of single-stranded DNA (ssDNA) breaks. PARP1 is over-expressed in a number of cancer types. PARP1 inhibitors prove highly effective therapies for cancers with BRCAness.
	PLK4	64	10	1	-1.316303546	65.86536923	50.79139009	0.019904268	Serine/threonine-protein kinase PLK4	PLK4 knockdown decreases *in vivo* growth of breast cancer xenografts. PLK4 inhibitor, CFI-400945, had single-agent antitumor activity *in vivo*, and induced significant regression of PTEN-null TNBC and colon cancer, suggesting PLK4 may be a PTEN-null therapeutic target.
	HDAC2	62	36	3	-1.68740977	2283.613283	1992.844976	4.62E-05	Histone deacetylase 2	HDAC2 is often significantly overexpressed in solid tumors; its inactivation resulted in regression of tumor cell growth and activation of cellular apoptosis.
	DHFR	64	10	1	-1.316303546	303.3643354	239.0140045	0.00019444	Dihydrofolate reductase	DHFR is essential for DNA precursor synthesis, thus it was the first enzyme to be targeted for cancer chemotherapy.
	MYO6	64	22	1	-2.52279368	7100.480743	5470.694425	0.006672326	Unconventional myosin-VI	MYO6 overexpressed in prostate cancer and multiple cancer types; MYO6 knockdown attenuates prostate cancer cell migration; shMYO6 reduced cell growth and increased apoptosis in colorectal cancer.
	NQO1	64	14	1	-1.824361347	1016.423495	752.4725285	0.012669247	NAD(P)H dehydrogenase [quinone] 1	NQO1 is expressed at high levels in numerous human cancers, including breast, colon, cervix, lung, and pancreas; NQO1 has potential as a therapeutic target for cancer therapy.
TP53 (Mutation)	CDK7	29	19	0	-11.94014085	517.6720103	453.7370643	0.009587173	Cyclin-dependent kinase 7	Triple-negative breast cancer (TNBC) cells are highly dependent on CDK7, and CDK7 inhibitor blocks tumor growth in TNBC PDX model; A covalent CDK7 inhibitor, THZ1, strongly reduces the proliferation and cell viability of T-ALL cell lines.
	RAD17	29	19	0	-11.94014085	626.6575414	594.3827793	0.084934618	Cell cycle checkpoint protein RAD17	Overexprssed in colon and breast cancer; Depletion of RAD17 sensitizes pancreatic cancer cells to gemcitabine.
	BDP1	29	18	0	-11.83157895	1013.501324	829.4167408	0.025936849	Transcription factor TFIIIB component B" homolog	High rates of Pol III transcription are necessary for cancer cells to sustain growth, and requires TFIIIB. BDP1 is a component of TFIIIB.
	GALNT3	29	13	0	-11.3	2594.882314	2168.29356	0.054622435	Polypeptide N-acetylgalactosaminyltransferase 3	GALNT3 overexpression in multiple cancers, including gastric, ovarian, pancreatic and lung. GALNT3 knockdown in epithelial ovarian cancer cells led to sharp decrease of cell proliferation, migration and invasion.
SMAD4 (Deletion)	NMT1	6	17	0	-10.33009709	2115.429033	1917.665085	0.026318219	Glycylpeptide N-tetradecanoyltransferase 1	NMT1 activity and protein expression were higher in human colorectal cancer, gallbladder carcinoma and brain tumors. NMT1 inhibition reduces cell proliferation and induces apoptosis in melanoma cell lines and also blocks tumor growth *in vivo*.
	ACLY	6	11	0	-10.20952381	9849.06285	8788.038608	0.064880591	ATP-citrate synthase	ACLY is upregulated or activated in several types of cancers, and its inhibition is known to induce proliferation arrest in cancer cells both *in vitro* and *in vivo*.
	XBP1	6	9	0	-10.170347	23601.68268	16697.94201	0.002389882	X-box-binding protein 1	XBP1 is activated in TNBC and has a pivotal role in the tumorigenicity and progression of this human breast cancer subtype; Depletion of XBP1 inhibited tumor growth and tumor relapse.
RB1 (Deletion)	MBD2	53	5	0	-10.96715328	1272.695374	1156.523888	0.034600109	Methyl-CpG-binding domain protein 2	MBD2 is a very attractive target for cancer prevention and treatment; Mbd2 deficiency dramatically reduces adenoma burden and extends life span in a gene dosage-dependent manner in mouse model.
	PATZ1	53	5	0	-10.96715328	1912.832768	1675.643638	0.005508321	POZ-, AT hook-, and zinc finger-containing protein 1	PATZ1 binds to other DNA binding structures to play an important role in chromatin modeling and transcription regulation; PATZ1 is overexpressed in colon carcinomas; Its silencing inhibits colon cancer cell proliferation or increases sensitivity to apoptotic stimuli of glioma cells; The development of B-cell lymphomas, sarcomas, hepatocellular carcinomas and lung adenomas in Patz1-knockout mice supports its tumor suppressor function.
	SKA1	53	4	0	-10.77090909	34.81816038	29.72090931	0.099886183	Spindle and kinetochore-associated protein 1	SKA1 is overexpressed in gastric cancer and promotes cell growth; SKA1 over-expression promotes prostate tumourigenesis; SKA1 is required for metastasis and cisplatin resistance of non-small cell lung cancer.

Gene *A* (*PTEN*, *TP53*, *SMAD4* and *RB1*) represents the most common altered tumour suppressors in prostate cancer. For each gene in the Gene *B* list the table shows: (1) mutual exclusiveness score (odds ratio score) with Gene *A*; (2) Gene *B* expression in Gene *A*-deleted prostate cancer samples ($P < 0.1$); and (3) proposed functions in cancer progression. *P* values were determined by two-tailed *t*-test.